

The rôle of metals in amyloid aggregation. Experiments and *ab initio* simulations

V. Minicozzi ^{a)}, S. Morante ^{a),b)1}, G.C. Rossi ^{a)}, F. Stellato ^{a)}
N. Christian ^{c)}, K. Jansen ^{d)}

^{a)} Dipartimento di Fisica, Università di Roma “Tor Vergata”
INFN, Sezione di Roma “Tor Vergata”

Via della Ricerca Scientifica, 00133 Roma, Italy

^{b)} CRS - SOFT c/o Dipartimento di Fisica - Università di Roma “La Sapienza”
P.le A. Moro, 00185 Roma, Italy

^{c)} Humboldt University, Theoretical Biophysics, Department of Biology
Invalidenstr. 42, 10115 Berlin - Germany

^{d)} NIC, DESY, Zeuthen, Platanallee 6, 15738 Zeuthen - Germany

ABSTRACT

With a combination of modern spectroscopic techniques and numerical first principle simulations it is possible to investigate the physico-chemical basis of the β -amyloid aggregation phenomenon, which is suspected to be at the basis of the development of the Alzheimer disease.

On the one hand, in fact, X-ray Absorption Spectroscopy can be successfully used to determine the atomic structure around the metal binding site in samples where β -amyloid peptides are complexed with either Cu^{2+} or Zn^{2+} ions. Exploiting spectroscopic information obtained on a selected set of fragments of the natural $\text{A}\beta$ -peptide ($\text{A}\beta_{1-40}$), the residues that along the sequence are coordinated to the metal are identified. While copper data can be consistently interpreted assuming that oligopeptides encompassing the minimal 1-16 amino acidic sequence display a metal coordination mode which involves three Histidines (His_6 , His_{13} and His_{14}), in complexes with Zn^{2+} a four Histidines coordination mode is seen to be preferred. Lacking a fourth Histidine in the $\text{A}\beta_{1-16}$ fragment, this geometrical arrangement hints to a Zn^{2+} promoted inter-peptide aggregation mode.

On the other hand, first principle *ab initio* molecular dynamics simulations of the Car-Parrinello type, which have proved to be of invaluable help in understanding the microscopic mechanisms of chemical bonding both in solid state physics and in structural biophysics, have been employed in an effort to give a theoretical basis and find a phenomenological interpretation of the available experimental data on $\text{A}\beta$ -peptides-metal complexes. Using medium size PC-clusters as well as larger parallel platforms, it is possible to deal with systems comprising 300 to 500 atoms and 1000 to 1500 electrons for simulation times as long as 2 ÷ 3 ps. We present structural results that nicely compare with NMR and XAS data.

¹Speaker

1 Introduction

The term amyloidosis refers to a family of pathologies in which endogenous proteins and peptides switch from the physiological soluble configuration to a pathological fibrillar insoluble state. They comprise a heterogeneous group of diseases (more than 20) which are characterized by “plaques” formation [1]. Plaques are found to contain fairly large amount [2, 3] of transition metals like Cu, Fe and Zn (the last one being the most abundant) whose function is not yet fully understood. The interest of elucidating the rôle of metals in amyloidosis development strongly increased after noticing that Cu and Zn chelators can be used to solubilize the $A\beta$ -aggregates [4, 5] which appear to make up the fibrillar material associated with the Alzheimer’s disease (AD).

Indeed the main proteinaceous component of the amyloid brain deposition, detected in patients affected by AD, is the so called amyloid β -peptide ($A\beta$ -peptide), which originates from the cleavage of a protein called Amyloid Precursor Protein (APP). The latter is a 770 amino acid (a.a.) long trans membrane protein coded in chromosomal 21. Various secretases are known to be able to cut APP [6]. If the pair of α and γ secretases is involved in the cutting event, the result is a non-pathological, harmless form of the peptide. On the contrary, when the cut is performed by the β and γ pair, the pathological, harmful $A\beta$ -peptide form of the protein is produced. The experimental evidence that $A\beta$ -peptides can form complexes with Cu^{2+} and Zn^{2+} ions has attracted a lot of interest from the scientific community. In particular there are indications that the two ions may play opposite functions, with Cu having an inhibitory effect on the Zn induced aggregation propensity [7].

1.1 The rôle of metals

Metals are essential cell components in all living species as they are required in many biochemical reactions. They are also involved in a large number of functions, and metal proteins represent about 30 % of all proteins [8, 9]. It is not surprising, therefore, that an unbalanced concentration of metals, either too high or too low, can result in severe threats to the organism. This is the reason why metal metabolism and trafficking (like uptake, delivery and removal) is accurately regulated in the cell.

It may be interesting to recall that the average total amount of Zn in human body is around $1.5 \div 2.5$ grams, while the total average amount of Cu is much lower, around $50 \div 100$ milligrams, but its importance is comparable or possibly higher than that of Zn [10, 11, 12].

The concentration of Zn is particularly high in certain specialized brain areas and it has been noticed that Zn metabolism is altered during diseases and physical stress. Besides copper and zinc, many other metals (like calcium, magnesium, manganese, iron, cobalt, and molybdenum) are involved in the metabolism of the Central Nervous System (CNS), as catalysts, second messengers, gene expression regulators, etc., and thus play an essential rôle in the correct functioning of the brain. Clearly metals must be supplied to the CNS in an optimally tuned way in order to prevent aberrant behaviour. The transport across the Blood Brain Barrier (BBB) is the first step in the regulation of their level in brain [13]. In this context it is interesting to note that high aluminum content is found in temporal cortex and hippocampus and Al has been demonstrated

to significantly alter the BBB permeability [14, 15, 16] and accelerate amyloid aggregation [17]. Furthermore its co-incubation with either Zn^{2+} or Cu^{2+} was shown to promote precipitation, but apparently without amyloid fibrils formation [18].

In the brain, metals like Cu, Zn and Fe, are normally present at fairly high concentration and there are evidences that a breakdown in metal trafficking regulation has a significant impact in the development of age-related neurodegenerative diseases [19, 20]. During neurotransmission processes high concentrations of Zn (at the level of $\sim 300 \mu\text{M}$) and Cu (at the level of $\sim 30 \mu\text{M}$) are normally released. Release of Cu and Zn has been considered as one of the cause of the precipitation process (which starts in the synapse) leading to amyloid aggregation [21]. As we mentioned above, the concentration level of these metals was found to be, in fact, especially high in amyloid plaque deposits, reaching 0.4 mM for Cu and 1 mM for Zn [2].

1.2 Experimental techniques

Many techniques have been used during the last decade to try to characterize the structure of the metal binding site in β -amyloid complexes, among which Electron Paramagnetic Resonance (EPR) [22], Nuclear Magnetic Resonance (NMR) [22, 23, 24], Circular Dichroism (CD) [24, 22] and X-ray Absorption Spectroscopy (XAS) [25, 26].

In this contribution we will concentrate on the XAS technique, as it displays a number of interesting features when it is employed in the study of biological systems, and especially in the study of metallo-proteins [27, 28, 29, 30, 31, 32]. Perhaps the most important of them is that XAS can be used for samples in any state of aggregation. A further advantage with respect to other spectroscopic approaches is that there are no selection rules that would extinct the signal in unlucky circumstances, with the result that a XAS signal is always present. Finally XAS is very sensitive to the nature of the metal absorber. It allows extracting structural information about the absorber atomic environment through the study of the oscillations of the absorption coefficient that originate from the interference between the outgoing wave of the electron (photoelectron) kicked-off from the absorber and the back-scattered waves emerging from the atoms surrounding it. This interference spectrum contains detailed information about scatterer-absorber relative positions, from which the geometrical and structural arrangement of the a.a.'s that are coordinated to the metal can be inferred with fairly good accuracy. Data analysis requires a rather sophisticated theory where single and multiple scattering (MS) contributions [33, 34] must be taken into account.

1.2.1 Cu-A β complexes

NMR studies of the Cu-A β_{1-16} complex [24] have suggested that the aromatic ring of Tyrosine₁₀ (Tyr₁₀) and the imidazole groups of His₆, His₁₃ and His₁₄ are likely to be involved in the coordination of the peptide with the metal ion. This finding is compatible with the XAS study performed on the Cu-A β_{1-40} complex [26].

Analysis of CD, EPR and NMR data [22] of the Cu-A β_{1-16} and Cu-A β_{1-28} samples hint, instead, at a geometrical structure where Cu is coordinated to the N-terminal nitrogen, besides the same three, His₆, His₁₃ and His₁₄, imidazole rings seen in the NMR experiments of ref. [24].

1.2.2 Zn-A β complexes

In the case of the Zn-A β_{1-16} complex the situation appears to be more complicated and several coordination modes have been proposed. In particular, NMR investigations [23] have suggested a variety of inter-molecular Zn binding geometries involving different numbers of Histidines together with the peptide N-terminus. The existence of these peculiar inter-molecular binding modes was confirmed by XAS studies [25] on the Zn-A β_{13-21} complex, in which pairs of peptides are found to be cross-linked by a Zn bridge anchored to two Histidines. In further NMR studies [35, 36] also an intrapeptide coordination mode where Zn²⁺ binds three Histidines and the N-terminus was proposed. The high variability of Zn coordination according to circumstances (concentration, preparation mode of the sample, etc.) has been also observed in recent XAS experiments on Zn-A β_{1-40} complexes [26, 37].

1.3 Recent XAS experiments

In this review we want to focus on the results of a thorough XAS study carried out on a selected set of fragments of the A β_{1-40} -peptide complexed with either Cu²⁺ or Zn²⁺ [37]. Beside confirming the general results of [26] concerning the existence of important structural differences between Cu and Zn coordination modes, these investigations were able to elucidate the special rôle played by the N-terminal region in binding the metal. In particular, it is found that only two Histidines residues are coordinated to Cu when the first four amino acidic residues are cut out (as is the case with the Cu-A β_{5-23} sample). It is natural to make the hypothesis that, among the three Histidine residues (His₆, His₁₃ and His₁₄) relevant in metal coordination, it is His₆ that is no more available for copper binding, because binding is hindered by the proximity of the dissociated N-terminus.

The situation with Zn-A β complexes is somewhat different. It is, in fact, observed that cutting out the first four amino acidic residues of the peptide does not modify the number of coordinated Histidine residues, as was the case for Cu complexes. The spectrum in the so called EXAFS (Extended X-ray Absorption Fine Structure) region remains unaltered and XAS results are in all cases compatible with four coordinated Histidine residues, indicating that each metal ion is shared by two A β -peptides. The presence of the first four amino acidic residues only affects the local geometry around the Zn absorber, as it is demonstrated by the markedly different structure of the XANES region (X-ray Absorption Near Edge Structure) of the spectrum of the Zn-A β_{5-23} sample with respect to that of all the others.

1.4 *Ab initio* simulations

Owing to the recent spectacular technical and architectural advances in the design of new high performance computers, extremely powerful platforms are today available to the scientific community which allow to attack problems of unprecedented complexity in many research fields ranging from high energy particle physics to disordered systems, from material science to systems of biological interest [38].

In this exciting and promising situation we have decided to set up a long term research project aimed at building up a flexible computational tool for first principle *ab initio* simulations especially aimed at dealing with biological macromolecules. Systems of interest in this research field are, however, extremely large (some 10^3 atoms and up to 10^4 electrons) and cannot be simulated in their full complexity and for adequately long times due to obvious CPU limitations. Thus a judicious modeling of the key features of the system is necessary and an intelligent compromise must be found between the need to have a sufficiently realistic model and the drawback of ending up with an impossibly large number of atoms and electrons.

In this contribution we wish to present a feasibility study and the first results of the *ab initio* simulations of the Car–Parrinello (CP) type ² that we have carried out in the paradigmatic example of $A\beta$ -metal complexes with the aim of performing a comparative study of copper and zinc structural coordination modes. The experience gained by our group in a previous similar study (we have investigated the Cu coordination mode in the prion protein (PrP) binding sites located within the N-terminal octarepeat region [42, 43]) and the availability of a fair amount of CPU time ³ have been the crucial ingredients that have allowed us to set up convenient models for the systems we wanted to investigate and obtain the first interesting results. The latter will be presented below in sect. 3.

The alternative road to CP simulations is that of using either quantum chemistry methods [49] or hybrid approaches, like QM/MM [50]. In general these methods have the virtue that they allow tackling model systems of almost realistic sizes. However, nothing is for free. The price to pay when using the first kind of approach is that one must know *a priori* the detailed atomic structure of the system, while in the second case one has to employ classical mechanics for a large portion of the system and set up a delicate matching procedure in the region of the system where quantum and classical mechanics will have an overlap.

Both the above strategies have been used for the investigation of the geometrical structure of the copper binding site in the PrP case. A non-exhaustive list of papers can be found in refs. [51, 52, 53, 54]. Not much has been done, instead, on the important issue of the specificity of transition metals binding properties in $A\beta$ aggregation processes.

1.5 Content

The content of this mini-review is the following. In sect. 2 we highlight the information obtained from a number of experimental techniques (XAS, Optical Density (OD) and Fourier Transform Infra-Red spectroscopy (FTIR)) concerning Cu and Zn coordination mode in situations where these ions are complexed with several different fragments of the $A\beta_{1-40}$ -peptide. In sect. 3 we describe the nature and the potentialities that *ab initio* simulations of the Car–Parrinello type offer for the understanding of the available

²Good reviews on the subject as well as references to the original paper [39] can be found in [40, 41].

³We had the opportunity of using many computer facilities, among which Cineca cluster [44] (Bologna - Italy), FermiI cluster [45] at E. Fermi Research Center (Roma - Italy), BEN cluster [46] at ECT* (Trento - Italy), CERM cluster [47] (Firenze - Italy) and ALTIX 4700 [48] at Leibniz-Rechen Zentrum (LKZ) (Munich - Germany).

Oligopeptide	a.a. sequence
$A\beta_{1-16}$	$H_3N^+-DAEFRHDSGYEVHHQK-COO^-$
$A\beta_{1-28}$	$H_3N^+-DAEFRHDSGYEVHHQKLVFFAEDVGSNK-COO^-$
$A\beta_{5-23}$	$H_3N^+-RHDSGYEVHHQKLVFFAED-COOH_3N^+$
$A\beta_{17-40}$	$H_3N^+-LVFFAEDVGSNKGAIIGLMVGGVV-COO^-$
$A\beta_{1-40}$	$H_3N^+-DAEFRHDSGYEVHHQKLVFFAEDVGSNKGAIIGLMVGGVV-COO^-$

Table 1: The amino acidic sequence of the five $A\beta$ oligopeptides considered in ref. [37].

experimental information and we present some preliminary results. Conclusions and an outlook of possible future lines of investigations can be found in sect. 4.

2 XAS experimental results

For the sake of comparing different physico-chemical situations the XAS spectra of a number of fragments of the $A\beta_{1-40}$ -peptide complexed with either Cu^{2+} or Zn^{2+} have been measured. These are the five oligopeptides whose sequence is reported in Table 1⁴. Actually the XAS data relative to the $A\beta_{1-40}$ -peptides were taken from [26].

These particular fragments of the $A\beta_{1-40}$ -peptide have been selected for a number of different reasons. $A\beta_{1-16}$ is the minimal fragment which contains all the three Histidines (His_6 , His_{13} and His_{14}) that have been suggested to be involved in metal binding, while $A\beta_{17-40}$ is the complementary sequence where none of these Histidines is present. In the $A\beta_{1-28}$ fragment, besides the presence of the three Histidines, a long hydrophobic region (see below) that is believed to be relevant in the aggregation processes is contained. The $A\beta_{5-23}$ fragment was considered with the main purpose of trying to answer the question whether the N-terminal region of the $A\beta$ -peptide can play any rôle in the metal binding process.

All the XAS data we will discuss here have been collected at the D2 bending magnet beam line of the EMBL Outstation Hamburg at DESY [55]. The X-ray spectra of the samples were recorded in fluorescence mode.

⁴Note that an H_3N^+ group appears also at the C-terminus of the $A\beta_{5-23}$ sample. The reason why we have this cap at the C-terminus of the $A\beta_{5-23}$ is that this peptide has been synthesized in loco using Solid-phase peptide synthesis (SPPS) technique. In order to avoid polymerization of amino acids protecting group are normally used. The general principle of SPPS is a repeated cycles of coupling-deprotection. The free N-terminal amine of a solid-phase attached peptide is coupled to a single N-protected amino acid unit. This unit is then deprotected, revealing a new N-terminal amine to which the successive amino acid may be attached and so on. At the end of the synthesis, that proceeds from C-terminus to N-terminus, the peptide is cleaved from resin, but the cleavage leaves an H_3N^+ group attached at the C-terminus. Avoiding C-terminus capping would require a much more expensive method which we could not afford. In any case capping of the C-terminus is even welcome in XAS experiments, as one does not want to have it reactive.

2.1 XAS data analysis

XAS spectra are normally analyzed by separating out the near edge region (the so-called XANES region) from the EXAFS region which extends from about 50 eV above the edge onward. In fact, the difficulty of getting a reliable theoretical description of the very complicated electronic processes affecting the low-energy part of the spectrum makes its quantitative interpretation especially problematic [56, 33, 57, 58, 59]. At the same time, however, the structure of this region of the spectrum is very sensitive to the electronic structure of the absorber and the symmetry of the local environment around it, and can yield valuable information on similarities and differences when relative local geometries of structurally similar samples are compared [34]. At variance with this situation, valuable quantitative structural information can be more easily extracted from the EXAFS part of the spectrum, even starting with limited knowledge on the atomic structural environment around the absorbing metal.

A general comparison of the XANES and EXAFS portions of the spectra of the 10 samples (5 fragments complexed with either Cu or Zn) that have been subjected to XAS measurements reveals an interesting pattern of strong similarities and differences that are summarized in the following Table where the equality sign means identity (within errors) of spectral features in the region under consideration.

- XANES

$$\begin{aligned} (\text{Cu-A}\beta)_{1-16} &= (\text{Cu-A}\beta)_{1-28} = (\text{Cu-A}\beta)_{1-40} \neq (\text{Cu-A}\beta)_{5-23} \neq (\text{Cu-A}\beta)_{17-40} \\ (\text{Zn-A}\beta)_{1-16} &= (\text{Zn-A}\beta)_{1-28} \neq (\text{Zn-A}\beta)_{1-40} \neq (\text{Zn-A}\beta)_{5-23} \neq (\text{Zn-A}\beta)_{17-40} \end{aligned}$$

- EXAFS

$$\begin{aligned} (\text{Cu-A}\beta)_{1-16} &= (\text{Cu-A}\beta)_{1-28} = (\text{Cu-A}\beta)_{1-40} \neq (\text{Cu-A}\beta)_{5-23} \neq (\text{Cu-A}\beta)_{17-40} \\ (\text{Zn-A}\beta)_{1-16} &= (\text{Zn-A}\beta)_{1-28} = (\text{Zn-A}\beta)_{1-40} = (\text{Zn-A}\beta)_{5-23} \neq (\text{Zn-A}\beta)_{17-40} \end{aligned}$$

The comparison of the XANES and EXAFS regions of the XAS spectrum of Cu and Zn complexes are shown in Figs. 1, 2, 3 and 4. It is worth noticing that the difference in the level of similarities of the XANES and EXAFS region among the various Zn samples is not a problem. Rather it should be interpreted as an evidence for the marked flexibility of the Zn^{2+} coordination [60]. In Figs. 1 and 2 only the XANES spectra of Cu- and Zn-A β complexes that show visibly different features among themselves are shown.

In view of the qualitative considerations emerging from the above figures and summarized in the previous Table, one can limit the discussion to the the EXAFS spectra of the following samples

1. (Cu-A β)₁₋₁₆, as a prototype of (Cu-A β)₁₋₁₆, (Cu-A β)₁₋₂₈ and (Cu-A β)₁₋₄₀ samples;
2. (Cu-A β)₅₋₂₃, as its EXAFS spectrum is different from that of the samples of the first group;
3. (Zn-A β)₁₋₁₆, as a prototype of all Zn complexes (with the exception of (Zn-A β)₁₇₋₄₀, see below).

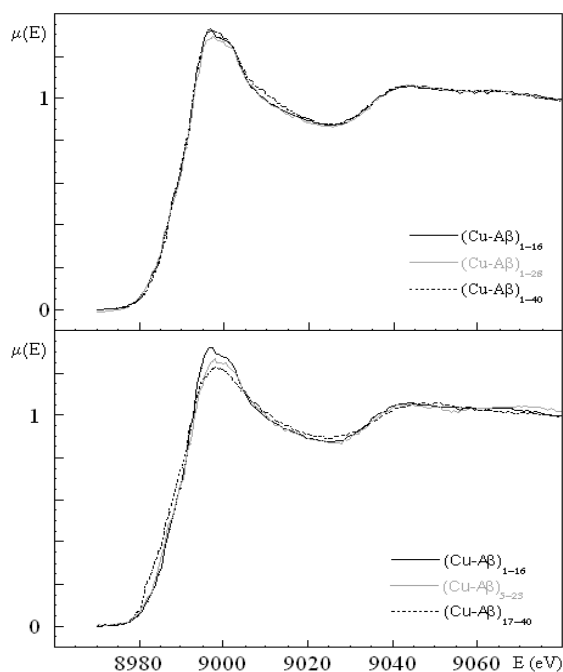


Figure 1: The XANES portion of the spectra of Cu-A β complexes. The figure is taken from ref. [37].

No fitting of the (Cu-A β)₁₇₋₄₀ and (Zn-A β)₁₇₋₄₀ data was carried out, because their EXAFS spectra are almost identical to that of the corresponding buffer solutions (data not shown). This similarity is very consistent with the idea that the metal is not bound to the 17-40 a.a. portion of the A β -peptide and in agreement with the absence of conformational change displayed in FTIR experiments (see ref. [37] for more details and Fig. 10 below).

2.2 Fitting strategy

Because of the lack of detailed structural information (no X-ray crystallographic data are available for A β -peptides), in fitting our XAS data we decided to follow the strategy advocated in [26], where it was proved that an efficient way to single out possible geometries needed to start the fitting procedure of the EXCURV98 package [61] is to extract them from Metallo-protein Database and Browser (MDB) [62]. In the fit the constrained refinement method suggested by [63] was followed, in which the His imidazole and the Tyr phenyl rings are treated as rigid bodies. Below we will refer to the N-imidazole and O atoms, through which His and Tyr are respectively bound to the absorber, as “leading atoms”. It is important to note here that, even if in general one cannot distinguish among light scatterers (like N, O and C) only on the basis of their individual contribution to the EXAFS signal, when acting as leading atoms they can be generally unambiguously identified because they are tightly anchored to a large and

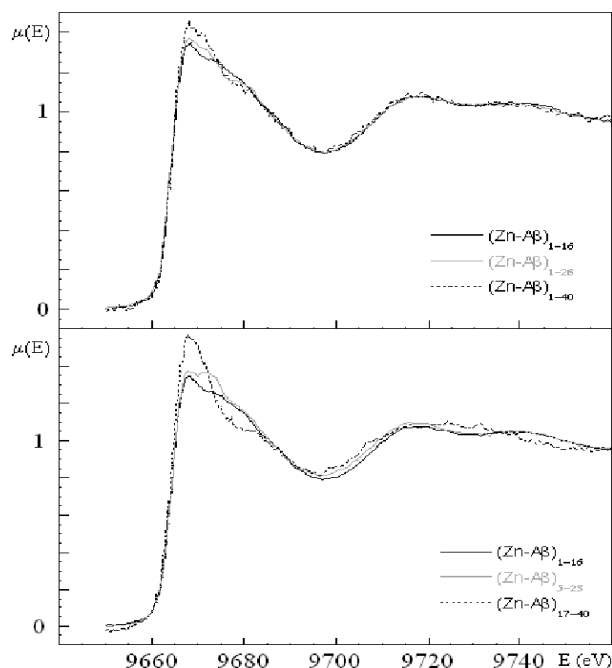


Figure 2: The XANES portion of the spectra of Zn-A β complexes. The figure is taken from ref. [37].

well ordered bunch of atoms.

Following the above ideas and exploiting indications coming from the literature [23, 24, 26, 36, 35], various initial geometrical models have been tried differing by the number of His's involved in the metal coordination. The best results of the fit to the data are discussed and presented in sects. 2.3 and 2.4. We now separately discuss results for copper and zinc complexes.

2.3 Cu complexes

For the reasons explained in sect. 2.1, only the EXAFS spectra of the (Cu-A β)₁₋₁₆ and (Cu-A β)₅₋₂₃ samples have been analyzed.

2.3.1 (Cu-A β)₁₋₁₆

In the upper panel of Fig. 5 the fitted (black line) and experimental (gray line) spectra of the (Cu-A β)₁₋₁₆ fragment are shown. The modulus of the Fourier Transform (FT) of both the experimental and theoretical spectrum is shown in the lower panel. The best fit parameters characterizing the atomic arrangement around the absorber are reported in Table 2 (see the Appendix for details on the meaning of the parameters reported in the Table). We remark that the distance r , refers to the position of the “leading atom” we have defined above. Oxygen atoms that are simply indicated with O in the Table, belong either to a water molecule or to a.a.'s other than a His or a Tyr. One

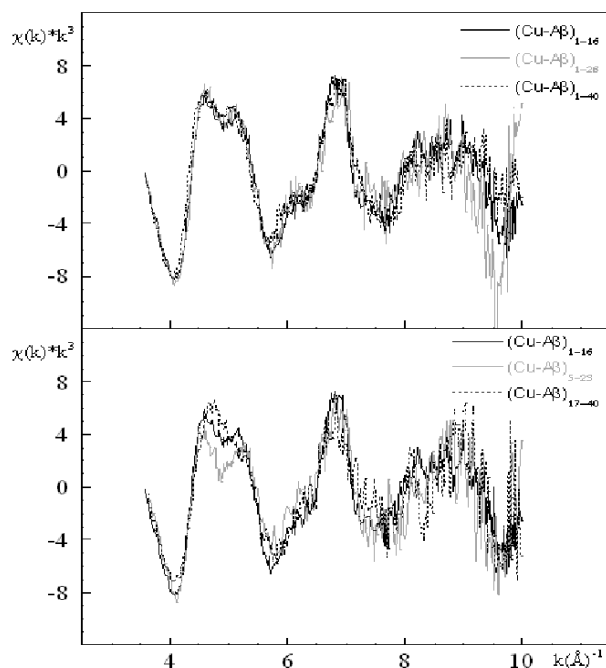


Figure 3: Comparison of the EXAFS portion of spectra of Cu complexes. The figure is taken from ref. [37].

finds that in the case of the $(\text{Cu-A}\beta)_{1-16}$ complex the best fit of Fig. 5 is obtained by including three His's and one Tyr in the coordination sphere of the metal, plus an oxygen atom possibly belonging to a water molecule or to an a.a. other than His or Tyr. This structure, whose PDB is sketched in Fig. 6, is exactly the one already proposed in [26] for the Cu environment in the case of the $(\text{Cu-A}\beta)_{1-40}$ peptide. One should notice that in the case of the $(\text{Cu-A}\beta)_{1-16}$, the model in which the Tyr oxygen is replaced by the nitrogen of the N-terminus, gives rise to a fit only marginally worse than the one whose structural parameters are reported in the Table. Consequently, on the basis of these fits one cannot completely rule out the possibility of a coordination with the N-terminal nitrogen. There have been, however, arguments in the literature that tend to exclude Tyr₁₀ as a Cu ligand [64, 65, 22, 66].

The situation one is facing here is an important example of a case where *ab initio* simulations can be of help in answering a crucial structural question. Namely, whether it is the Tyr oxygen or the N-terminal nitrogen which is coordinated to copper. We will take back this point in sect. 3.

2.3.2 $(\text{Cu-A}\beta)_{5-23}$

Moving to the $(\text{Cu-A}\beta)_{5-23}$ sample, a fit starting from the best previously identified structural model for $(\text{Cu-A}\beta)_{1-16}$ was first tried. A satisfactory fit could not be obtained by taking the coordinated residues to be the same as in the previous sample and

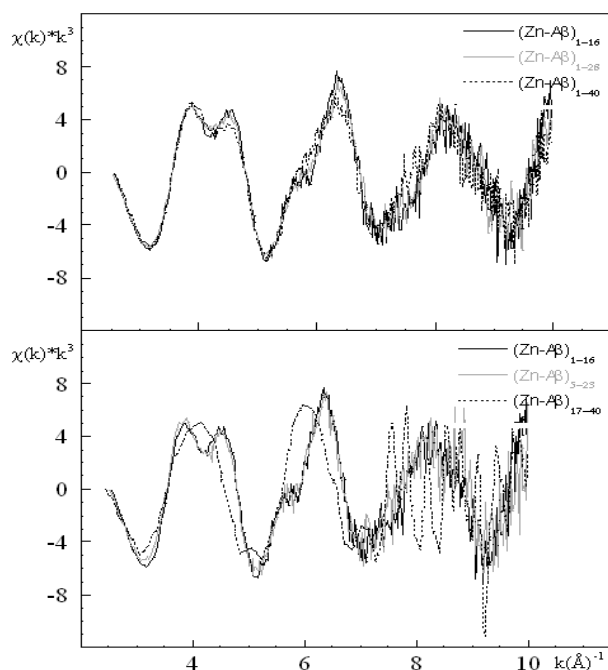


Figure 4: Comparison of the EXAFS portion of the spectra of Zn complexes. The figure is taken from ref. [37].

only modifying their geometrical parameters. A geometrical configuration, inspired by the work of [64] was then tried, in which His₆ is replaced by the N-terminal amino group. In this model Cu²⁺ is coordinated to two Histidines, one Tyrosine, the nitrogen belonging to the N-terminal amino group, and one oxygen atom. A fairly satisfactory fit is obtained in this way (Fig. 7). A sketch of the geometrical structure of the metal environment is shown in the central panel of Fig. 6.

It must be remarked that, despite the nice appearance of the fit, its quality factor (the so called *R*-factor, see Appendix) is poorer ($R \sim 40\%$) than in the previous (Cu-Aβ)₁₋₁₆ case ($R \sim 28\%$). These *R* values are, however, consistent with the fact that the signal-to-noise ratio was lower for (Cu-Aβ)₅₋₂₃ than for (Cu-Aβ)₁₋₁₆ EXAFS data. The validity of this interpretation was checked by subjecting the (Cu-Aβ)₅₋₂₃ data to a simple smoothing procedure which consists in averaging over sets of nearby experimental points. In this way an almost exactly identical set of best fit parameters is obtained but with a significantly reduced *R*-factor ($R \sim 30\%$). As already mentioned in the Introduction, the fact that, by cutting out the first four amino acidic residues, the number of coordinated Histidines passes from three to two, is a strong indication that it is His₆ the third bound Histidine, because one expects that the decreased flexibility of the initial part of the peptide will prevent His₆ (at the second position in the Aβ₅₋₂₃-peptide) to come in contact with the metal.

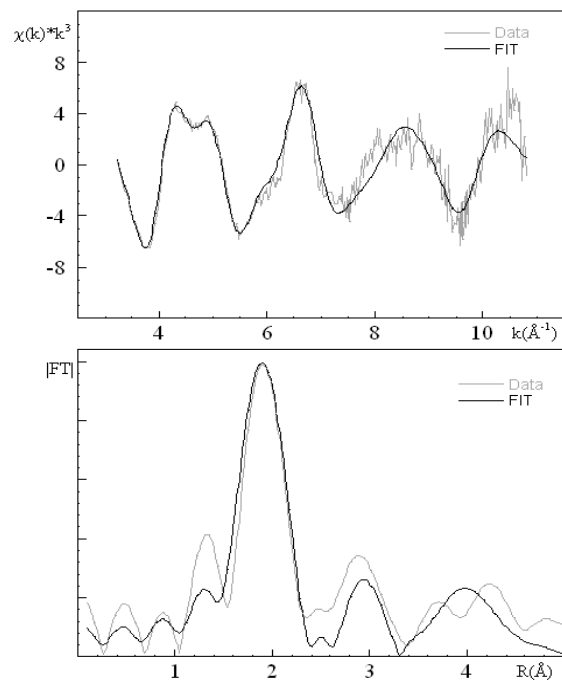


Figure 5: Fit to the $(\text{Cu-A}\beta)_{1-16}$ EXAFS spectrum. The figure is taken from ref. [37].

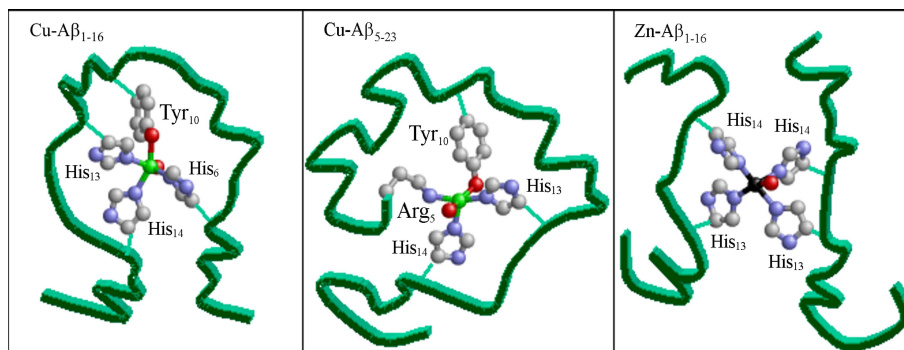


Fig. 8

Figure 6: An artistic view of the metal environment. Left panel refers to the $(\text{Cu-A}\beta)_{1-16}$ complex, central panel to the $(\text{Cu-A}\beta)_{5-23}$ complex and right panel to the $(\text{Zn-A}\beta)_{1-16}$ complex. The figure is taken from ref. [37].

Coordinated residue	N	$r \pm \Delta r$ Å	$\sigma^2 \pm \Delta\sigma^2$ Å ²
(Cu-Aβ)₁₋₁₆			
His	3	1.95 ± 0.01	0.002 ± 0.001
Tyr	1	1.95 ± 0.01	0.002 ± 0.001
O	1	2.06 ± 0.01	0.002 ± 0.001
$\Delta E_F = -10.2 \pm 0.7$ eV $R = 28\%$			
(Cu-Aβ)₅₋₂₃			
His	2	1.99 ± 0.01	0.003 ± 0.001
Tyr	1	1.99 ± 0.01	0.003 ± 0.001
N (terminus)	1	1.99 ± 0.01	0.003 ± 0.001
O	1	2.27 ± 0.01	0.003 ± 0.001
$\Delta E_F = -13.8 \pm 0.4$ eV $R = 40\%$			
(Zn-Aβ)₅₋₂₃			
His	2	1.96 ± 0.01	0.003 ± 0.001
His	2	2.00 ± 0.01	0.003 ± 0.001
O	1	2.00 ± 0.01	0.003 ± 0.001
$\Delta E_F = -6.5 \pm 0.2$ eV $R = 23\%$			

Table 2: The best fit parameters characterizing the atomic arrangement around the absorber. First and second columns show type and number, N , of coordinated chemical groups (atom or residue); third and fourth column, distance, r , from the absorber to the coordinated atom or to the leading atom of the coordinated residue and corresponding value of Debye-Waller (DW) factors, σ^2 . Errors for distances and DW factors are written next to each parameter. For each sample the Fermi energy shift, ΔE_F , and the quality factor, R , of the fit are reported in the last row.

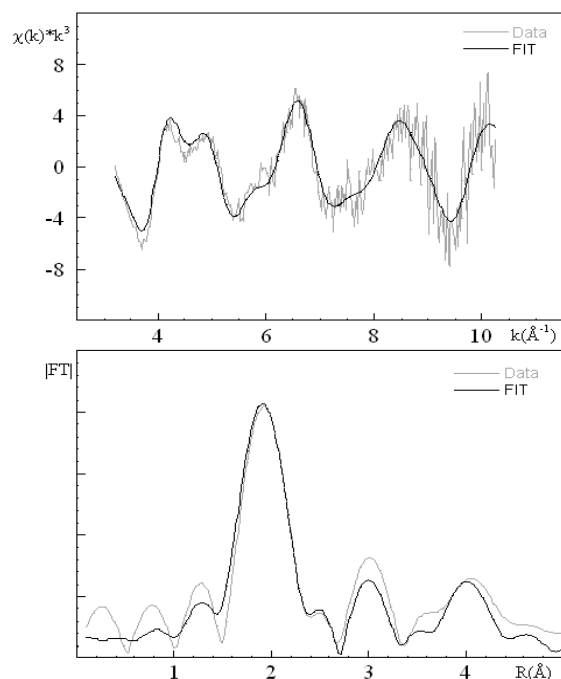


Figure 7: Fit to the $(\text{Cu-A}\beta)_{5-23}$ EXAFS spectrum. The figure is taken from ref. [37].

2.4 Zn complexes

2.4.1 An observation

Before going through the analysis of Zn^{2+} complexes, it should be mentioned that data collected in [26] have shown that solution and pellet Zn preparations lead to very different structural arrangements around the metal. In that paper it was also argued that in the solution preparation chlorine ions (present at fairly high concentration because HCl was used to adjust the pH in the Tris buffer used in the experiments) are able to come sufficiently near to Zn to be detectable. Since chlorine ions are certainly not present at such an high concentration in physiological conditions, in [37] NEMO (and not Tris) was used as a buffer. As expected, this modification affects Zn^{2+} , but not Cu^{2+} , data. In fact, no appreciable modification of the whole XAS spectrum of $(\text{Cu-A}\beta)_{1-40}$ is visible when comparing the old data obtained with the Tris buffer to the data where the NEMO buffer is employed.

The situation is rather different for the $(\text{Zn-A}\beta)_{1-40}$ complex, as data collected when the latter was dissolved in the NEMO buffer [37] are definitely different from those collected in [26] where the Tris buffer was used. For the comparative study between Cu and Zn complexes the $(\text{Zn-A}\beta)_{1-40}$ data of ref. [37] should be employed as they are more homogeneous to those of the Cu complexes and nearer to physiological solution conditions.

Just like in the case of Cu complexes, the EXAFS spectra (see Fig. 4) of (Zn-

$A\beta$)₁₋₁₆, (Zn- $A\beta$)₁₋₂₈ and (Zn- $A\beta$)₁₋₄₀ are all equal within errors, while the (Zn- $A\beta$)₁₇₋₄₀ sample shows a spectrum almost identical to that of Zn^{2+} in buffer (data not shown). These facts taken together confirm that the absence of the first 16 amino acidic residues prevents metal binding to occur. However, at variance with Cu complexes, here also the EXAFS spectrum of (Zn- $A\beta$)₅₋₂₃ is very similar to the spectrum of the three Zn samples comprising the first four a.a.'s of the $A\beta$ -peptide sequence, namely (Zn- $A\beta$)₁₋₁₆, (Zn- $A\beta$)₁₋₂₈ and (Zn- $A\beta$)₁₋₄₀.

Above the difference of the (Cu- $A\beta$)₅₋₂₃ EXAFS spectrum with respect to that of the other Cu complexes was attributed to the absence of the Cu-His₆ coordination bond. From this observation and the strong similarity of the EXAFS spectra of the four Zn complexes (Zn- $A\beta$)₁₋₁₆, (Zn- $A\beta$)₁₋₂₈, (Zn- $A\beta$)₁₋₄₀ and (Zn- $A\beta$)₅₋₂₃, one can conclude that in all Zn samples His₆ is never involved in metal coordination (obviously His₆ is not even present in (Zn- $A\beta$)₁₇₋₄₀). As a prototype of the above four (almost) identical Zn complex spectra, only the (Zn- $A\beta$)₁₋₁₆ EXAFS have been subjected to a quantitative analysis.

2.4.2 (Zn- $A\beta$)₁₋₁₆

In order to fit the XAS spectrum of the (Zn- $A\beta$)₁₋₁₆ sample, a set of initial models was chosen according to the strategy illustrated above in sect. 2.3. In particular, various starting geometrical structures from MDB [62] database have been selected among those having the desired number of Histidine residues bound to the metal. When necessary, the geometry of the initial atomic configuration was manually adjusted to better match available experimental information. The best fit, shown in Fig. 8, is obtained by including four Histidines and one oxygen in the Zn^{2+} coordination sphere. A sketch of the Zn environment obtained after fitting the data of the (Zn- $A\beta$)₁₋₁₆ complex is shown in right panel of Fig. 6.

The existence of this peculiar structure (with four Histidines coordinated to the metal) is of the utmost relevance from a structural point of view and it is perhaps the most interesting outcome of the experimental investigation described in this review. Recalling, in fact, that each $A\beta$ -peptide only contains three Histidines, the result illustrated above means that in order for the metal to be coordinated to four Histidines, at least two different peptides must be involved in the Zn^{2+} binding mode.

The conclusion of this analysis gives support to the idea that Zn^{2+} is able to bind to $A\beta$ -peptides in a much less rigid way than Cu^{2+} . This finding is in agreement with the results reported in [26], where it was shown that the number of Histidines coordinated to Zn^{2+} in the (Zn- $A\beta$)₁₋₄₀ complex, is correlated to the procedure employed in the sample preparation.

2.5 Optical density and FTIR measurements

Visible differences in metal binding modes between Cu and Zn are confirmed by complementary OD and FTIR experiments [37], which also suggest that the type of metal coordination is correlated with the metal ability of promoting aggregation (Fig. 9) and secondary structure switching (Fig. 10).

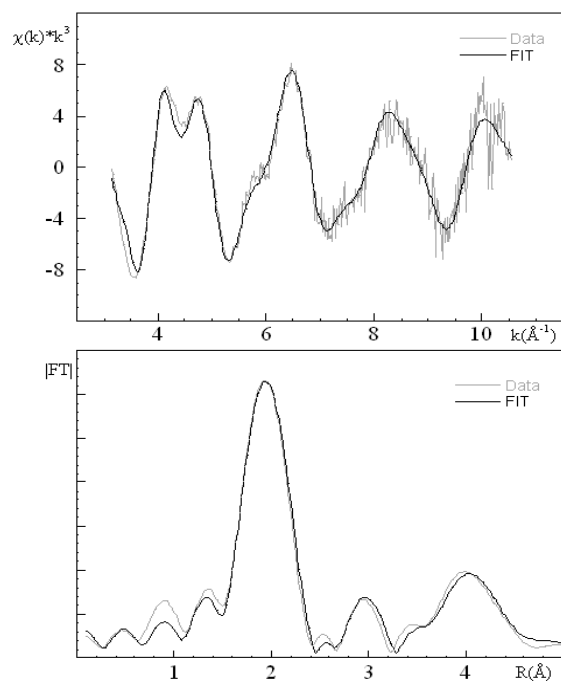


Figure 8: Fit to the $(\text{Zn-A}\beta)_{1-16}$ EXAFS spectrum. The figure is taken from ref. [37].

2.5.1 Optical density measurements

In Fig. 9 the percentages of aggregation for the 5 samples of Table 1, as measured in OD experiments are reported using a self-explanatory bar code. For each peptide three different preparations are subjected to OD measurements, namely the peptide dissolved in the buffer in the absence of any metal (left bar) and the peptide dissolved in the buffer in the presence of $70 \mu\text{M Me}^{2+}$, where Me^{2+} is either Cu^{2+} (middle bar) or Zn^{2+} (right bar). As a general feature, we see that in the absence of metal none of the samples show signs of aggregations within error bars. Furthermore it is confirmed that the percentage of aggregation is not zero within errors in the presence of metal ions, with Zn being more effective than Cu, and that the percentage of aggregated peptide is significantly higher for $\text{A}\beta_{1-40}$ than for all the other peptides [37].

2.5.2 FTIR measurements

FTIR can give useful information on the conformational arrangement of peptides. In the absence of metals, the FTIR spectra of $\text{A}\beta_{1-28}$, $\text{A}\beta_{5-23}$, $\text{A}\beta_{1-40}$ and $\text{A}\beta_{17-40}$ show a peak (Fig. 10) in a wave-number region typical of a β -sheet secondary structure, corresponding to $k \sim 1630 \text{ cm}^{-1}$, while for the $\text{A}\beta_{1-16}$ sample the peak is at a wave-number $k \sim 1654 \text{ cm}^{-1}$, typical of an α -helix structure. When Cu is present a conformational change from β -sheet to α -helix secondary structure is expected. Actually a quite pronounced conformational change in the case of $\text{A}\beta_{1-40}$ and $\text{A}\beta_{1-28}$

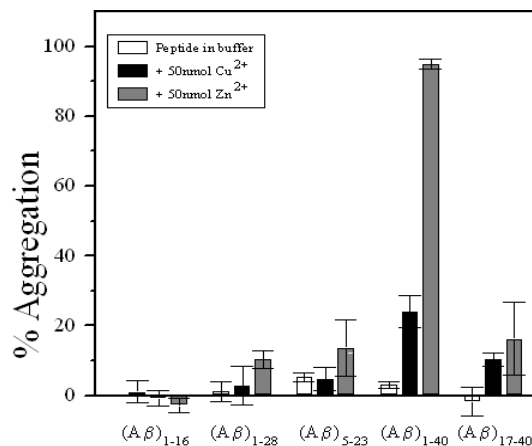


Figure 9: OD data. The figure is taken from ref. [37].

is observed, signaled by the fact that the characteristic FTIR peak moves toward the wave-number typical of an α -helix structure.

A similar shift does not occur in the case of the $A\beta_{17-40}$ and $A\beta_{5-23}$ fragments. In the case of $A\beta_{17-40}$ this fact may be taken as an indication that Cu does not bind to the peptide, possibly as a consequence of the fact that all Histidines are removed from it. As for the $A\beta_{5-23}$ fragment, the situation is more subtle. In [37] the absence of a structural change was not attributed to the fact that Cu does not bind to the peptide, but rather to the circumstance that, owing to the structural stress induced by the absence of the first 4 a.a.'s, His₆ is not anymore bound to the metal. In other words FTIR measurements are suggestive for a special rôle played His₆ in determining the secondary structure switch induced by copper. Of course nothing special happens to the $A\beta_{1-16}$ fragment, which is in an α -helix secondary structure even in the absence of Cu. Despite its stronger aggregating activity, Zn has almost no effect on peptide conformation. This is consistent with the hypothesis [23] according to which Cu is mainly involved in intra-peptide binding (with conformational change), whereas Zn promotes inter-peptide binding, hence, possibly aggregation (with no conformational changes).

2.6 Summary of experimental results

Detailed XAS measurements on fragments of various length of the $A\beta_{1-40}$ -peptide in complex with either Cu or Zn have been collected and analyzed with the aim of determining the precise position and the local atomic structure of the metal binding site.

Putting together the results of various complementary experimental techniques, it can be concluded that an intra-peptide type of coordination mode is visible in Cu- $A\beta$ -fragment complexes with the metal bound to the three Histidines (His₆, His₁₃ and His₁₄) and possibly Tyr₁₀ giving rise to a rather rigid and stable peptide structure (see left panel in Fig. 6).

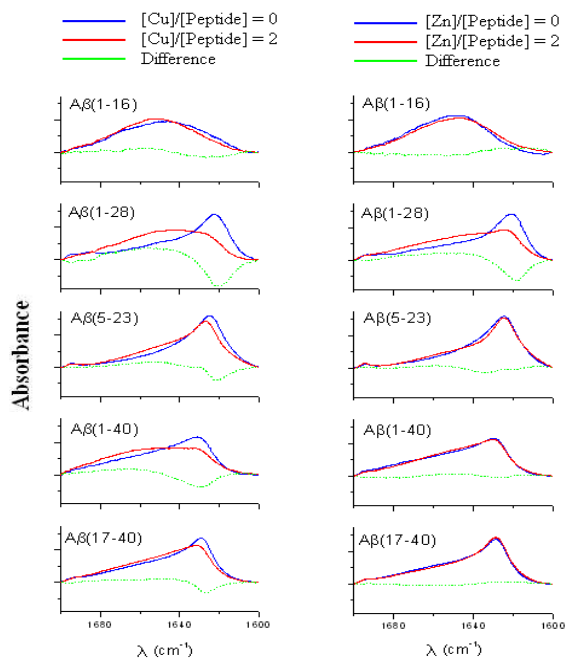


Figure 10: FTIR data. The figure is taken from ref. [37].

Results concerning Zn complexes indicate instead, in agreement with suggestions coming from the work of [23], that in the presence of zinc a network of A β -peptides is formed with the metal stabilizing the structure by binding Histidines (from two to four, see also [67]) belonging to adjacent peptides. This structural arrangement points towards a propensity of Zn to form more flexible and open coordination geometries, hence to promote β -amyloid aggregation.

The great complexity of the experimental landscape that emerges from the analysis we presented in this mini-review was a strong motivation for enlarging our research interests in the direction of trying to get an understanding of the atomic basis of the key steps that are at the root of misfolding and aggregation processes. Along these lines the development of a ready-to-use and technically advanced know-how (algorithms and codes) aimed at dealing with *ab initio* simulations of large and structured systems is necessary. We then started a long-term project with the aim of setting up a general strategy for quantum mechanical “first principle” simulations of the CP type for systems with $O(10^3)$ degrees of freedom, the first steps of which have been published in refs. [42, 43]. Further applications to the case of A β -peptides are discussed and reported in the next section.

3 Car–Parrinello Molecular Dynamics simulations

In this part of the review we want to discuss how *ab initio* simulations (in particular “Car–Parrinello Molecular Dynamics” (CPMD) simulations) can be profitably used to

interpret experimental results and possibly discriminate among different models thanks to the detailed atomic information that numerical methods can provide.

CPMD simulations have been largely and very successfully used in many research areas ranging from solid state physics to biological systems. Among the numerous papers in these areas, see for instance those quoted in refs. [68] and [54], respectively. As we said, in applications to metal–protein complexes CPMD was employed and validated in a detailed structural study of the copper binding sites located in the unstructured octarepeat region of PrP [42, 43].

3.1 The pro’s and con’s of CPMD simulations

The use of quantum mechanical (QM) methods (as opposed to purely classical MD approaches) for computing the force field felt by atoms is mandatory in the study of metal–protein complexes for two reasons. One is of a technical nature and has to do with the presence of a metallic (doubly charged) ion in the system, which makes much safer the use of first principle simulations, as they embody charge polarization and screening, rather than the use of classical MD which would require employing one of the rather sophisticated, but still not fully satisfactory, algorithmic tricks that have been developed to deal with the situation where the long range Coulomb interactions are present [69]. The second reason is more fundamental and it is related to the fact that it is the main purpose of any structural study to identify the nature of metal ligands. This is of course something which is not known *a priori* and should be the main outcome of the investigation rather than an input as would be the case if one decides to employ classical atomic force fields. We wish to mention, however, that there have been interesting classical MD simulations of stacks of β -amyloid peptides (in the absence of metals) which confirm experimental indications [70] about the peculiar way in which in their early stage of aggregation peptides may be packed and structured [71].

An obvious limitation to the use of quantum-mechanical numerical simulations is the foreseeable very short length of the CPMD trajectory (few picoseconds for systems of the size one is interested in here) which certainly can never be as extended as one would like it to be. However, in the light of the drawbacks of using classical MD described above, one may still decide to use QM methods accepting the practical limitations that go with this methodological choice. A possible way to cope, at least partially, with the difficulties related to the conflict between the need to deal with a realistically large system and the consequent limitations concerning the length of the simulated trajectory could be to exploit the possibilities offered by the recently developed mixed classical/quantum-mechanical methods, like QM/MM [50]. For lack of space we will not discuss this possibility any further in this review.

In any case there are good reasons (supported by a quite long experience in the field of CPMD simulations) which make one to believe that already a few picosecond trajectory can give useful information on structural problems like those we are dealing with here (i.e. identification of primary metal ligands). The argument is based on the observation that CPMD simulations can be thought of as a way of successively computing the electronic density while atoms move slowly around. From this perspective CPMD may be considered not so terribly different from genuine DFT or quantum chemistry computations [49], provided one can live with the two well known problems

of the CPMD method. Namely, the fact that excited electronic states are essentially inaccessible and that atoms will only be able to explore a region of the phase space not too distant from their initial configuration.

It is interesting to note that the application of CPMD methods to the problem at hand here is not set back by any of these two limitations. In fact, what one wants to identify and characterize are the possibly different coordination modes of zinc and copper ions when complexed with various portions of the $A\beta_{1-40}$ peptide. Indeed one is only interested in understanding what could be the specific rôle of these metals just in the very first steps of a possible aggregation process, where equilibrium is not yet an issue. This more modest approach is still of great relevance because it looks that only the compounds that are formed in the very early stages of the aggregation process are pathological. The subsequent steps of mesoscopic fibril formation may on the contrary have a protective effect against neurodegenerative processes [72]-[74]. In any case it is driven by an extremely complicated dynamics which at the moment is beyond any possible atomistic description.

Two further issues remain to be discussed. One is the choice of the initial configuration for the successive CPMD simulations. The second is the extent to which the method is capable of performing an exhaustive exploration of the system phase space. Both problems are of the greatest importance, but in this special case are fairly well kept under control because the system configurations from which CPMD simulations are started off are taken from experimental structural data (NMR, EPR, XAS). Furthermore one is in the rather favourable situation where the very compact arrangement, detected in experiments (see Fig. 11 taken from ref. [36]), that the system takes in the presence of metals, significantly reduces the magnitude of the actually accessible phase space.

3.2 The ESPRESSO package for CPMD simulations

A parallel version of the freely available Quantum-ESPRESSO package (opEn-Source Package for Research in Electronic Structure, Simulation, and Optimization [75, 76]) which incorporates Vanderbilt ultra-soft pseudo-potentials [77] and the PBE exchange-correlation functional [78] was used for all the CPMD simulations discussed in this section. Electronic wave functions were expanded in plane waves up to an energy cutoff of 25 Ry, while a 250 Ry cutoff was used for the expansion of the augmented charge density in the proximity of the atoms, as required by the ultra-soft pseudo-potential scheme. The choice of ultra-soft pseudo-potential was dictated by the fact that the light atoms of our systems, namely hydrogen, nitrogen, oxygen, carbon, would have required an impossibly high cutoff when standard norm conserving pseudo-potentials are employed [77].

To minimize finite volume effects periodic boundary conditions are imposed to the system. This choice has the extra bonus that the resulting geometry is well suited for plane wave expansion. The molecule is inserted in a supercell (filled with water molecules at 1 gr/cm³ density) with sufficiently large linear dimensions to ensure a separation between nearest replicas of the system to have negligible spurious electrostatic self-interactions. For neutral systems a separation of $4.5 \div 5$ Å is considered to be sufficient. For charged systems a separation of at least 8 Å is required.

CPMD calculations have been performed under spin-restricted conditions. This approximation is adequate for the kind of systems we are interested in this review, where only a single metal ion is present at the time. In a previous work [42] the realm of applicability of this simplified computational approach was studied with the conclusion that the effect of the spin polarization is negligible and can become relevant only when more than one metal ion are simultaneously present.

3.3 Setting up the simulated model systems

As we said, the main goal of the CPMD simulations we are going to present is to investigate, in the important instance of $A\beta$ -peptides, the rôle played by metallic ions (specifically copper and zinc) in giving the protein its functionality or, on the contrary, in transforming it into a pathogenic conformer.

There exist in the literature somewhat conflicting results about the Cu coordination modes in $A\beta$ -peptides. On the one hand, in fact, NMR data on copper complexed with $A\beta_{1-28}$ [22] and $A\beta_{1-40}$ [36] peptides suggest that three Histidines (His_6 , His_{13} and His_{14}) are coordinated to the metal with the fourth ligand being a nitrogen from the N-terminus. On the other, XAS experiments on various portions of the natural $A\beta_{1-40}$ protein [26, 37] and NMR/EPR experiments on the $A\beta_{1-28}$ peptide [79], as well as NMR data on the $A\beta_{1-16}$ [24] fragment, all point to the conclusion that, besides the same three Histidines, the fourth copper ligand is the Tyr_{10} oxygen. In this context it should be remarked that, as we work at $\text{pH}=7$, it is an open question (which simulations can possibly clarify) whether the Tyr hydroxyl radical can really be deprotonated when binding a metal in view of the fact that $\text{pK}(\text{Tyr})=10.9$ [80].

Clarifying the metal coordination mode in the various instances is not without interest, because it is expected that the more or less open structure of the peptide can strongly influence its aggregation propensity. Typically one may suspect that a coordination mode where the N-terminus is not bound to Cu will give rise to a more open geometry, which would probably be more prone to aggregation.

We have thus set up three specific model systems (termed S_1 , S_2 and S_3 in the following) for CPMD simulations to try to elucidate some of the above points. As we explained, the detailed structure of the models we have set up is the result of the compromise between the need of having a sufficiently realistic description of the actual physical system and the impossibility of dealing with too many atoms and electrons. According to this criterion we have built up the simulated systems as follows. First of all we have decided to limit our attention to the $A\beta_{1-14}$ segment (see Table 1) where the copper binding site is known to be located. Secondly, since, as recalled above, the three Histidines, His_6 , His_{13} and His_{14} have been positively identified as Cu ligands, they are all explicitly included with their full atomic detail. As for the other a.a.'s, we have considered somewhat different choices for S_1 , S_2 and S_3 , as detailed below.

3.3.1 • S_1 •

- Of the a.a.'s from 1 to 6, besides their backbone, only the lateral chains of Asp_1 , Glu_3 and His_6 are retained. Among the remaining a.a.'s (from 7 to 14) only His_{13} and His_{14} are included in the model.

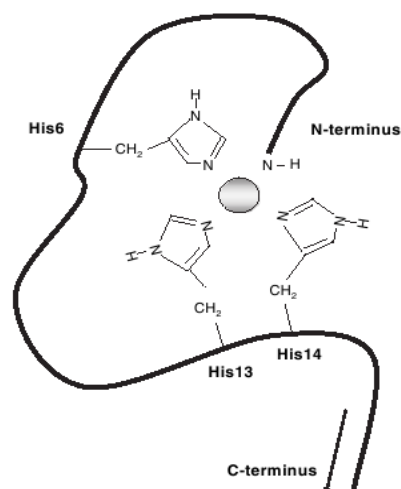


Figure 11: Sketch of N-terminal region of the $A\beta_{1-40}$ peptide. The figure is adapted from ref. [36].

- The C-terminus is capped in the usual way (i.e. by an $NHCH_3$ group), while the N-terminus of the fragment is left open (with an ending NH_2 group) to allow for possible Cu binding with loss of the amine hydrogen. The His_{13} - His_{14} dipeptide is capped with a CH_3CO group at its N-terminus and again by an $NHCH_3$ group at its C-terminus.

- The system, solvated with 125 water molecules, is contained in a box of volume $V=14 \times 19 \times 19 \text{ \AA}^3$. In this way density is equal to 1 g/cm^3 . Periodic boundary conditions are used and the size of the box has been chosen in such a way that the nearest copies of the same atom are separated by 5 \AA .

- The whole system is neutral as the double positive charge of Cu^{+2} is balanced by the sum of the negative charges of Asp_1 and Glu_3 .

- All in all, the total number of atoms of the system (including copper and water molecules) is 494, while that of electrons is 1369.

- The initial peptide configuration for the CPMD simulations has been taken from the PBD file of ref. [35] with Cu replacing Zn.

3.3.2 • S_2 •

- The backbone of the whole peptide is retained together with the lateral chains of Asp_1 , His_6 , Tyr_{10} , Glu_{11} , His_{13} and His_{14} .

- The C-terminus is capped in the usual way (i.e. by an $NHCH_3$ group), while the N-terminus of the fragment is left open (with an ending NH_2 group) to allow for possible Cu binding with loss of the amine hydrogen.

- The system, solvated with 225 water molecules, is contained in a box of volume $V=22 \times 23 \times 20 \text{ \AA}^3$. In this way density is equal to 1 g/cm^3 . Periodic boundary conditions are used and the size of the box has been chosen in such a way that the nearest copies

of the same atom are separated by 5 Å.

- The whole system is neutral as the double positive charge of Cu^{+2} is balanced by the sum of the negative charges of Asp_1 and Glu_{11} .

- All in all, the total number of atoms of the system (including copper and water molecules) is 838, while that of electrons is 2311.

- The initial configuration for the CPMD simulations has been taken from a 8 ns long classical MD simulation of the whole (Cu-A β)1 – 16 peptide in water with His_6 , His_{13} , His_{14} and Tyr_{10} bound to Cu. For this step the package GROMACS [81] was used.

3.3.3 • S_3 •

- The backbone of the whole peptide is retained together with the lateral chains of Asp_1 , His_6 , Tyr_{10} , Glu_{11} , His_{13} and His_{14} .

- The C-terminus is capped in the usual way (i.e. by an NHCH_3 group), while the N-terminus of the fragment is left open (with an ending NH_2 group) to allow for possible Cu binding with loss of the amine hydrogen.

- The system, solvated with 223 water molecules, is contained in a box of volume $V=20 \times 24 \times 20 \text{ \AA}^3$. In this way density is equal to 1 g/cm^3 . Periodic boundary conditions are used and the size of the box has been chosen in such a way that the nearest copies of the same atom are separated by 5 Å.

- The whole system is neutral as the double positive charge of Cu^{+2} is balanced by the sum of the negative charges of Asp_1 and Glu_{11} .

- All in all, the total number of atoms of the system (including copper and water molecules) is 832, while that of electrons is 2295.

- The initial configuration for the CPMD simulations has been taken from a 6 ns long classical MD simulation of the whole (Cu-A β)1 – 16 peptide in water with His_6 , His_{13} , His_{14} and the N-terminus are bound to Cu. For this step the package GROMACS [81] was used.

We notice that systems S_2 and S_3 are very similar. The only difference is in the fact that in the first case together with His_6 , His_{13} , His_{14} , Tyr_{10} is within a binding distance from Cu, while in the second case it is the peptide N-terminus which is initially near to Cu. Furthermore, since CPMD simulations are started from configurations taken after some few ns MD, the numbers of water molecules needed to fill the volume at unit density are slightly different for the two systems. This is because the elongation of the two peptides, and hence the volume they occupy, are slightly different (we recall that we want to have a fixed separation of 5 Å between adjacent images of the peptide in order to avoid unphysical interactions). For reader's convenience we sketch in Figs. 12 the initial atomic structure of the model systems S_1 , S_2 and S_3 .

3.3.4 Starting CPMD

Given the foreseeable very short duration of CPMD simulations (certainly not more than 10 ps), it is of the utmost importance to control the bias which is introduced by the choice of the initial atomic configuration from which the CP dynamics is started. Thus it is mandatory to start from either by some available PDB data (like the ones obtained

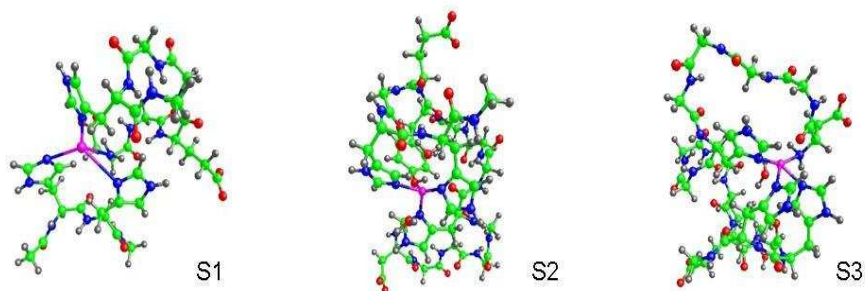


Figure 12: The atomic structure of the S_1 , S_2 and S_3 model systems. Colours are as follows: gray is H, red is O, green is C, blue is N and magenta is Cu.

in crystallography or NMR) or, lacking any such information, from some accurately equilibrated and thermalized configuration with the purpose of avoiding (or at least minimizing) biases and instabilities.

To cope with this problem we have started our CPMD simulations of system S_1 from the NMR data provided by ref. [35] (simply replacing Zn with Cu). For the systems S_2 and S_3 a different strategy was used. Namely it was decided to take as the initial structures for the successive CPMD simulations the configurations resulting after running very long (few ns) classical MD simulations. For this purpose preliminary very long MD simulations using GROMACS [81] were carried out for the S_2 and S_3 systems, until equilibration at 300 K was reached. The collected trajectories were 8 ns and 6 ns long, respectively. In Fig. 13 the stability of energy as a function of time can be appreciated.

In the present instance a further important question is to decide whether His₆, His₁₃, His₁₄ are bound to Cu through N_δ or N_ε. Unfortunately there is no full agreement in the literature. We report in Table 3 the most recent experimental findings on this issue, together with the choice made in the recent theoretical investigations of refs. [84, 85] and by our group. Similarly conflicting indications come from the structures collected in the MDB [62] database.

At this point, guided by the experience we acquired in our previous work [42], we have proceeded to minimize stresses and strains among atoms while electrons were adiabatically pushed to vanishing temperature, exploiting the numerical facilities available in the ESPRESSO code. After these preparatory maneuvers, the actual CPMD simulation can be started. More in detail the general protocol which we are following in our CPMD simulations consists in the four sequential steps briefly described below.

1. Minimization of electronic energy with fixed atomic positions.

ref.	year	metal	technique	His ₆	His ₁₃	His ₁₄
[82]	2001	Cu	EPR	N _ε	N _ε	N _ε
[22]	2004	Cu	EPR	N _ε	N _ε	N _ε
[79]	2005	Cu	EPR	N _ε	N _ε	N _ε
[24]	2006	Cu	NMR	N _δ	N _δ	N _δ
[35]	2006	Zn	EPR	N _δ	N _ε	N _δ
[83]	2007	Cu	NMR	N _ε	N _ε	N _ε
[36]	2007	Cu and Zn	NMR	N _ε	N _ε	N _δ
[84, 85]	2005, 2007	Cu	DFT+MD	N _δ	N _δ	N _δ
this work	2007	Cu	CPMD	N _δ	N _ε	N _δ

Table 3: In the first and second column we report the reference and the year in which the experiment was done. In the third column we indicate the employed experimental technique and in the fourth whether Cu or Zn complexes were considered. In the fifth, sixth and seventh column we specify the type of nitrogen atom bound to His₆, His₁₃, His₁₄, respectively. In the last two lines the choices made in the theoretical works are reported.

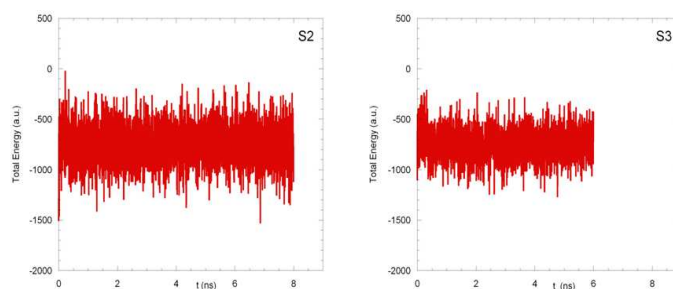


Figure 13: The energy history of classical MD simulations of the S_2 and S_3 model systems.

2. Minimization of total energy as a function of both atomic and electronic degrees of freedom of the full system.
3. Two (or more according to need) short (from 0.25 to 0.6 ps) preliminary sequential CPMD simulations at increasing atomic temperatures, using a Nosé–Hoover thermostat [86] coupled to atomic degrees of freedom, and kept at the desired temperature.
4. The final CPMD simulation of appropriate length at an atomic temperature of 300 K, using the same thermostat as in 3.

Thermalization in step 3. is necessary to slowly attain room temperature, thus avoiding that temperature oscillations affect in an uncontrolled way the approach of electrons to their ground state. The velocity-Verlet algorithm [87] for integrating the CP equations of motion was used with a time step of 0.12 fs.

3.4 Feasibility studies

We have first carried out a preliminary detailed feasibility study on the possibility of simulating the system S_1 on different platforms. We have tried the two PC-clusters and the large parallel machine whose characteristics are specified here below.

- Fermi1 Linux-clusters (E. Fermi Institute, Rome - Italy) based on 1.7 GHz Pentium IV processors [45].
- BEN Linux-cluster (ECT* Institute, Trento - Italy) based on Intel/Xeon-28 GHz processors [46],
- ALTIX 4700 (LKZ, Munich - Germany) based on Intel Itanium2 Madison 9M 1.6 GHz processors [48].

Estimated CPU times for a 1.2 ps long CPMD simulation (with a time step of 0.12 fs, this corresponds to 10^4 simulation steps) are given in Table 4 for a 16 node configuration. Though these numbers refer to the S_1 system, we have checked that within a factor of two they are also representative of the CPU simulation times required for the larger S_2 and S_3 systems.

Looking at Table 4 we see that, although not completely unreasonable, that CPU times attainable on PC-clusters would prevent a comfortable study of the metal coordination mode, as a thorough investigation would require (for each system) at least a factor of five more CPU time (thus something like about one to two year of full running) in order to allow for electron minimization, atomic equilibration and a CP simulation of say 4 ps. The conclusion of these considerations is that in practice it not possible to run our model systems on a medium-size PC-clusters.

Fortunately we had the chance of carrying out a study of the scaling of CPU times with the number of nodes for the same model system on the ALTIX 4700 computer. In its present configuration (9728 nodes) the machine is capable of attaining a peak performance of 62.3 Teraflops. We have run on it exactly the same system S_1 we tried on Fermi1 and BEN clusters, obtaining the scaling plot shown in Fig. 14. The gain in using the ALTIX machine is really remarkable. When we compare the performances summarized in Table 4, we see that not only ALTIX in its 16 node configuration is about 4 to 5 time faster than BEN or Fermi1, but the nice scaling of CPU times with the number of

Platform	CPU hours for 10^4 steps
Fermil in a 16 node config.	1650
BEN in 16 a node config.	1300
ALTIX in a 16 node config.	300

Table 4: CPU time in hours for a 10^4 step CPMD trajectory (corresponding to 1.2 ps real time) for the A β -peptide model system S_1 , comprising 494 atoms and 1369 electrons.

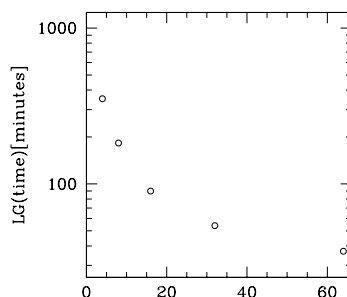


Figure 14: The scaling of the ALTIX 4700 CPU time with the number of nodes. The vertical axis is in minutes.

nodes (up to 64 nodes, see Fig. 14) may be profitably exploited to significantly speed up the simulations. With the conservative choice of a 64 node configuration one can attain computational times that allow to produce 10^4 steps (1.2 ps) in only 120 hours. Since these estimates are expected to be similarly good for the complexes where copper is replaced by zinc, we conclude that the whole research project of comparing copper and zinc structural properties in A β -complexes is perfectly feasible in a reasonable amount of time.

3.4.1 The size of the model systems

Before presenting our preliminary results, we wish to add a few comments on the crucial question concerning the size of the systems we have begun to simulate. In our opinion the models we have set up for the study of Cu-A β complexes capture rather well the essential features of the structural atomic arrangement around the metal ions suggested by experiments (mostly NMR and XAS).

Comparison of simulation data of systems S_1 with the more realistic S_2 and S_3 will also give us information about the reliability of the downsizing of the real A β -peptide system we have been obliged to make.

Of course one can be worried by the fact that for practical reasons our model systems display more or less simplified structures with respect to the full solvated (Cu-

$A\beta)_{1-16}$ complex. Thus we would like to give arguments to further support the kind of approach that we have decided to follow.

1) First of all we must stress that the preparatory classical MD simulations carried out to provide the initial starting configurations for the S_2 and S_3 CPMD simulations have been performed using the whole solvated $(Cu-A\beta)_{1-16}$ complex modeled in its full atomic detail. It is only when we move to CPMD simulations that the two systems are “reduced” to the models described in sects. 3.3.2 and 3.3.3.

2) The “reduced” systems we have set up are certainly not that small on the scale of what has been done in the literature in the framework of CPMD simulations or DFT computations. Rather, to our knowledge, they are among the largest ever tried.

3) In any case it is our intention to complement and extend QM computations with simulations based on QM/MM. By treating with classical mechanics the outer part of the peptide and the solvent, while leaving for a quantum mechanical treatment only the nearest environment around the metal, one will be able to explore more thoroughly the interesting part of the $(Cu-A\beta)_{1-16}$ phase space and for longer simulation times.

3.5 Some preliminary results

We report in this section the first few results we got from our classical and CPMD simulations for the three systems we have set up for the study of the conformational properties of $Cu-A\beta$ complexes.

3.5.1 The S_1 system

Starting from the atomic configuration suggested by the NMR experiments of ref. [35] (with Cu replacing Zn), a thermalization step consisting of two simulations of 0.6 ps at 100 and 200 K was first carried out for the system S_1 . After that, a CP trajectory 1.4 ps long at room temperature (300 K) was collected.

• **Results** – The main result of the simulation is that, starting from a configuration where, besides the imidazole rings of His₆, His₁₃ and His₁₄, the nitrogen of the N-terminus was lying within the Cu coordination sphere, the system ended up in a state where only the three Histidine remained coordinated to copper, while the N-terminal nitrogen was moving far out from it. This feature is clearly visible comparing Figs. 15 and 16, where as functions of time (for completeness also the history of the initial thermalization steps is reported) the distances from copper of the nitrogen atom of the N-terminus and of N_δ, N_ε and N_δ of the imidazole rings of His₆, His₁₃ and His₁₄, respectively, are displayed. From the figures it is clearly seen that the N-terminal nitrogen moves quickly away from copper reaching a distance of about 7 Å at the end of our simulation.

One might suspect that this result is the consequence of a distorted non-planar geometry around Cu. Actually this is not so. We report in fig. 17 the time history of the dihedral angle N_δ(H₆)–Cu–N_ε(H₁₃)–N_δ(H₁₄) from which it is clearly seen that after some initial time the system relaxes and oscillates around a configuration where the bound nitrogens around Cu are in a planar geometry.

Thus our preliminary simulations on the system S_1 do not seem to confirm the conclusions drawn from their NMR measurements in refs. [22] and [36], according to

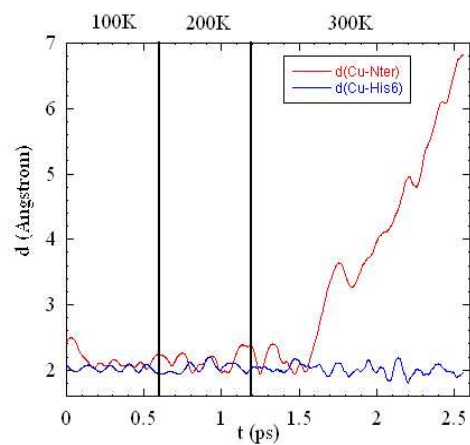


Figure 15: The time history of the distance from Cu of $N_{\delta}(\text{His}_6)$ (blue curve) and of the N-terminal nitrogen (red curve).

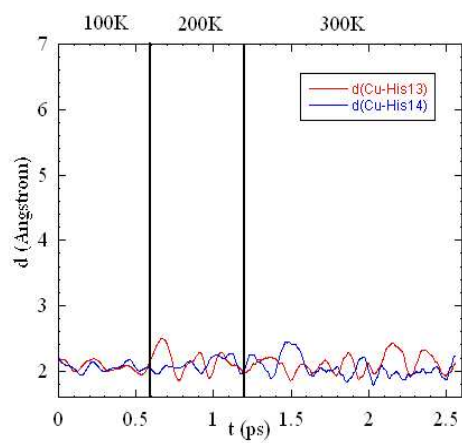


Figure 16: The time history of the distance from Cu of $N_{\epsilon}(\text{His}_{13})$ (red curve) and $N_{\delta}(\text{His}_{14})$ (blue curve).

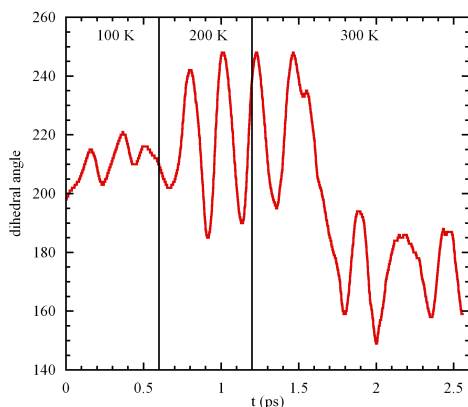


Figure 17: The dihedral angle $N_{\delta}(H_6)-Cu-N_{\epsilon}(H_{13})-N_{\delta}(H_{14})$ as a function of the CP simulation time.

which the N-terminal nitrogen is one of the Cu ligand.

- CPU-time requirement – The whole quantum-mechanical part of the CPMD simulation performed on the S_1 system was carried out on a 64 node configuration of the ALTIX 4700 supercomputer and took ~ 300 CPU hours for a total of about 20000 CPMD steps. This means something like 20000 hour/node. CPU times of this kind are very reasonable and can easily allow us to go on extending the length of the existing S_1 trajectory and moving to the simulation of the related (but larger) S_2 and S_3 systems.

3.5.2 The S_2 and S_3 systems

In order to cross-check this conclusion we decided to move to the more realistic systems S_2 and S_3 with the purpose of comparing the two situations where either the N-terminus (S_2) or the oxygen of Tyr₁₀ (S_3) is coordinated to Cu at the initial step of their respective CPMD simulations. The possibility that the Tyr₁₀ oxygen is the fourth Cu ligand was suggested in ref. [24] and confirmed in refs. [26, 37].

The study of systems S_2 and S_3 is in a very preliminary stage. At the moment we have finished with classical MD simulations and produced well equilibrated initial atomic configurations usable for the successive CPMD simulations. With these configurations we have started the long procedure described in sect. 3.3.4, finishing steps 1. and 2.

Even at this preliminary stage systems S_2 and S_3 already show some interesting difference. Namely, despite the fact that at the very beginning of the classical MD simulations $N_{\delta}(H_6)$, $N_{\epsilon}(H_{13})$ and $N_{\delta}(H_{14})$ were located in the same positions around Cu in both systems, after finishing classical MD and gone through the atomic energy minimization step of ESPRESSO, quite different geometrical arrangements are reached. In fact, Figs. 18, 19 and 20, which refer to system S_3 , show that a planar geometry

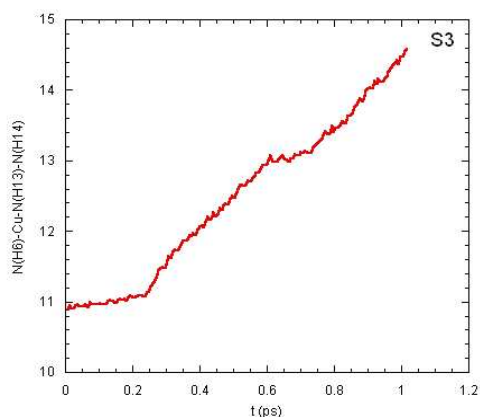


Figure 18: The behaviour of the dihedral angle $N_{\delta}(H_6)\text{-Cu-N}_{\epsilon}(H_{13})\text{-N}_{\delta}(H_{14})$ during the atomic energy minimization step of the system S_3 . The horizontal axis is the number of steepest descent steps.

around Cu, similar to the one we saw in the case of the S_1 system (see Fig. 17), is established for the four initially bonded atoms (N-terminus nitrogen, $N_{\delta}(H_6)$, $N_{\epsilon}(H_{13})$ and $N_{\delta}(H_{14})$). The situation looks completely different in the case of the S_2 system, where the dihedral angle $N_{\delta}(H_6)\text{-Cu-N}_{\epsilon}(H_{13})\text{-N}_{\delta}(H_{14})$ is always far from 180° (see Fig. 22).

We might thus expect to see that during the successive quantum-mechanical step of the CPMD simulation the N-terminus nitrogen will leave the Cu coordination sphere in the case of the S_3 system, as happened in the S_1 case. The question remain opens whether the initially Cu coordinated Tyr_{10} will remain within a bonding distance from the metal or not in the case of the system S_2 .

4 Conclusions and outlook

Although we are still far from a clear understanding of the rôle of metals in protein misfolding and/or aggregation, experimental and theoretical studies seem to point to a rather complex structural scenario.

In the instance of PrP it has been shown [29] that copper binding to the octarepeat region favours aggregation, possibly owing to an intermediate dimer formation mechanism [42], with the opposite being true when Cu binding occurs in the PrP core region [53].

In the case of $A\beta$ -peptides experimental information [26, 37] again point to a marked different behaviour depending on whether copper or zinc is involved in the game. While Cu is bound in a rather packed and stable configuration, Zn binding is more flexible and seems to be able to give rise to networks of cross-linked peptides [23].

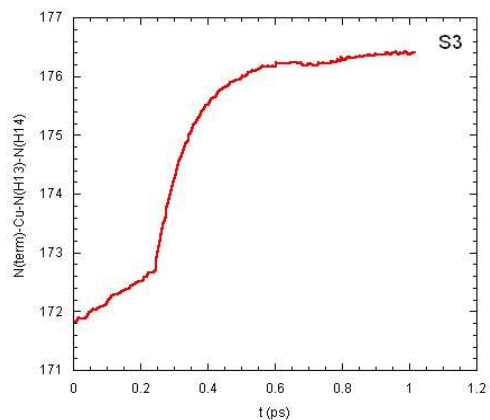


Figure 19: The behaviour of the dihedral angle N-terminus–Cu–N_ε(H₁₃)–N_δ(H₁₄) during the atomic energy minimization step of the system S_3 . The horizontal axis is the number of steepest descent steps.

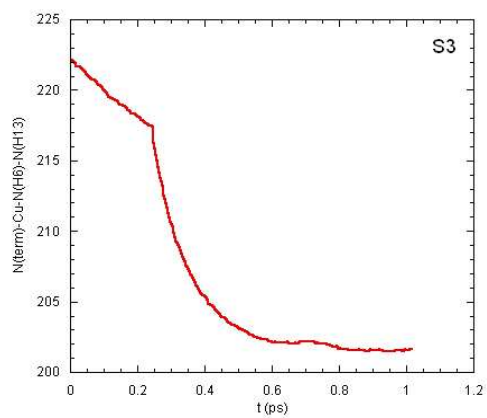


Figure 20: The behaviour of the dihedral angle N-terminus–N_δ(H₆)–Cu–N_ε(H₁₃) during the atomic energy minimization step of the system S_3 . The horizontal axis is the number of steepest descent steps.

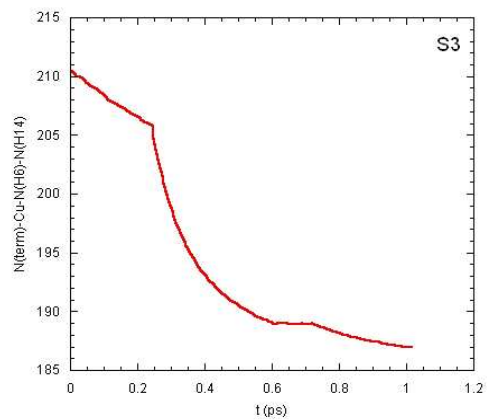


Figure 21: The diehedral angle N-terminus– $N_{\delta}(H_6)$ –Cu– $N_{\epsilon}(H_{14})$ during the atomic energy minimization step of the system S_3 . The horizontal axis is the number of steepest descent steps.

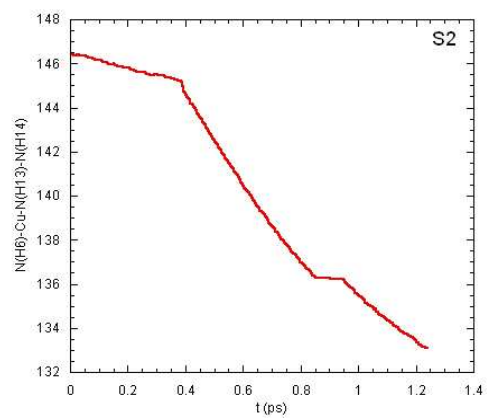


Figure 22: The behaviour of the diehedral angle $N_{\delta}(H_6)$ –Cu– $N_{\epsilon}(H_{13})$ – $N_{\delta}(H_{14})$ during the atomic energy minimization step of the system S_2 . The horizontal axis is the number of steepest descent steps.

From the theoretical point of view, numerical simulations of the Cu complexes have just started and at the moment it is premature to try to draw any conclusion from the numerical data that have been collected. In addition comparison with simulations where Cu is replaced by Zn must be carried out to enlight similarities and differences in the metal binding modes. It may well be that residues other than the ones we have included in the Cu model systems described above can come into play when we will move from Cu- to the less known Zn-complexes. There are indications [23] that Glu₁₁ or Asp₇ may also be relevant in this case. Of course, if necessary, models will be appropriately modified and tailored to fit the available experimental information.

Obviously adequately long and accurate numerical investigations are necessary before we can have a satisfactory interpretation of the existing experimental data. However, we are in this moment in the very lucky situation in which, thanks to the spectacular development in computer design and the ongoing continuous progresses in the implementation of innovative algorithmic softwares, reliable *ab initio* studies of structural properties of macromolecules are really within our reach in a few years from now. Indeed, with a foreseeable forthcoming scaling up of the available CPU times by some 10³ factor, one can hope to be soon able to simulate systems of biological interest of realistic size and for physical times of the order of the nanosecond.

Acknowledgments

We wish to thank S. Furlan, F. Guerrieri and G. La Penna for many fruitful discussions. Use of Cineca cluster (Bologna - Italy), Fermi1 cluster at E. Fermi Research Center (Roma - Italy), BEN cluster at ECT* (Trento - Italy), CERM cluster (Firenze - Italy) and ALTIX 4700 at LKZ (Munich - Germany) is gratefully acknowledged. Last but not least, a warm thank is also due to the Organizers of the Cetraro Workshop 2007 for the lively atmosphere of the Meeting.

Appendix

In this Appendix we recollect few standard formulae useful to clarify some of the symbols used in the text.

- The so-called EXAFS signal, $\chi(k)$, is defined through the measured total absorption coefficient, $\mu(E)$, and the absorption coefficient of the isolated absorber, $\mu_0(E)$, via the relation

$$\chi(k) = \frac{\mu(E) - \mu_0(E)}{\mu_0(E)}, \quad \hbar k = \sqrt{2m(E - E_0)}, \quad (1)$$

where m is the electron mass, \hbar the (reduced) Planck constant and k the wave vector of the extracted electron. k is related to the incident photon energy, E , and the ionization energy, E_0 , as shown in eq. (1).

- For completeness and to fix the notation we recall how the parameters introduced in Table 2 enter the theoretical formula representing the EXAFS signal. For simplicity we report equations valid in the single scattering approximation. In this case the

theoretical EXAFS signal has the expression

$$\chi(k) = S_0^2 \sum_{\ell} \frac{N_{\ell}}{kr_{\ell}^2} |f_{\ell}(k, \pi)| \sin(2kr_{\ell} + \phi_{\ell}(k)) e^{-\sigma_{\ell}^2 k^2} e^{-2r_{\ell}/\lambda(k)}, \quad (2)$$

where the sum over ℓ runs over the different coordination shells around the absorber. N_{ℓ} is the number of scatterers of the ℓ -th shell, located at a distance r_{ℓ} from the absorber and σ_{ℓ}^2 is the associated Debye-Waller factor. $|f_{\ell}(k, \pi)|$ is the modulus of the back-scattering amplitude and $\phi_{\ell}(k)$ the total scattering phase. Finally S_0^2 is an empirical quantity that accounts for all the many-body losses in photo-absorption processes and $\lambda_{\ell}(k)$ is the photo-electron mean free path. For MS processes a formally similar expression can be derived, in which r_{ℓ} represents the length of the full MS path. Modulus and phase functions have now more complicated expressions which depend on all the scattering events occurring along the MS path [33, 56, 57, 58, 59].

- The quality R -factor of a fit is computed as follows

$$R = \sum_{i=1}^P \frac{1}{w_i} |\chi^{\text{exp}}(k_i) - \chi^{\text{th}}(k_i)| \quad (3)$$

where $\chi^{\text{exp}}(k_i)$ and $\chi^{\text{th}}(k_i)$ are the experimental and theoretical data points, respectively, and the sum is over the number, P , of the k values at which data were collected. The “weighting” parameter w_i is defined by the formula

$$w_i = \frac{1}{k_i^n} \sum_{j=1}^P k_j^n |\chi^{\text{exp}}(k_j)| \quad (4)$$

where the integer n is selected in such a way that the amplitude of the EXAFS oscillations in the combination $k^n |\chi^{\text{exp}}(k)|$ does not die away at large values of k . In the analysis presented in this work the value $n = 3$ was taken.

As for the value of R , it is a consolidated experience that for complex biological molecules a fit can be considered adequately good when R falls in the interval between 20% and 40% [61].

References

- [1] Pepys, M.B. Philos Trans R Soc Lond B Biol Sci 2001, 356, 203-210.
- [2] Lovell, M.A.; Robertson, J.D.; Teesdale, W.J.; Campbell J.L.; Markesbery, W.R. J Neurol Sci 1998, 158, 47-52.
- [3] Smith, M.A.; Harris, P.L.; Sayre, L.M.; Perry, G. Proc Natl Acad Sci USA 1997, 94, 9866-9868.
- [4] Cherny, R.A.; Atwood, C.S.; Xilinas, M.E.; Gray, D.N.; Jones, W.D.; McLean, C.A.; Barnham, K.J.; Volitakis, I.; Fraser, F.W.; Kim, Y.S.; Huang, X.; Goldstein, L.E.; Moir, R.D.; Lim, J.T.; Beyreuther, K.; Zheng, H.; Tanzi, R.E.; Masters, C.L.; Bush, A.I. Neurol 2001, 30, 665-676.

- [5] Opazo, C.; Barria, M.I.; Ruiz, F.H.; Inestrosa, N.C. *Biometals* 2003, 16, 91-98.
- [6] Gandy, S. *J of Clinical Investigation* 2005, 115, 1121-1129.
- [7] Suzuki, K.; Miura, T.; Takeuchi, H. *Biochem Biophys Res Commun* 2001, 285, 991-996.
- [8] Lu, Y.; Valentine, J.S. *Curr Opin Struct Biol* 1997, 7, 495-500.
- [9] Jensen, M.R.; Hass, M.A.S.; Hansen, D.F.; Led, J.J. *Cell Mol Life Sci* 2007, 64, 1085-1104.
- [10] Linder, M.C. *The Biochemistry of Copper*; Plenum Press: New York, 1991.
- [11] Gaggelli, E.; Kozlowski, H.; Valensin D.; Valensin, G. *Chem Rev* 2006, 106, 1995-2044.
- [12] Zatta, P.; Frank, A. *Brain Research Review* 2007, 54, 19-23.
- [13] Zheng, W.; Aschner, M.; Ghersi-Egea, J.F. *Toxicol Appl Pharmacol* 2003, 192, 1-11.
- [14] Banks, W.A.; Kastin, A.J.; Zatta, P. The blood-brain barrier in aluminum toxicity and Alzheimer's disease, pp. 1-12, in *Non-neuronal cells in Alzheimer disease*, Zatta, P. and Nicolini, M. Eds.; World Scientific, Singapore, 1995.
- [15] Yokel, R.A. *Environ Health Perspect (suppl.)* 2002, 5, 699-704.
- [16] Bala Gupta, V.; Anitha, S.; Hedge, M.L.; Zecca, L.; Garruto, R.M.; Ravid, R.; Shankar, S.K.; Stein, R.; Shanmugavelu, P.; Jagannatha Rao, K.S. *Cell Mol Life Sci* 2005, 62, 143-158.
- [17] Drago, D.; Folin, M.; Baiguera, S.; Tognon, G.; Ricchelli, F.; Zatta, P. *Journal of Alzheimer's Disease* 2007, 11, 33-44.
- [18] Khan, A.; Ashcroft, A.E.; Korchazhkina, O.V.; Exley, C. *Journal of Inorganic Biochemistry* 2004, 98, 2006-2010.
- [19] Bush, A.I. *Trends Neurosci* 2003, 26, 207-214.
- [20] Barnham, K.J.; Masters, C.L.; Bush, A.I. *Nat Rev Drug Disc* 2004, 3, 205-214.
- [21] Therry, R.D. *J Neuropathol Exp Neurol* 1996, 55, 1023-1025.
- [22] Syme, C.D.; Nadal, R.C.; Rigby, S.E.J.; Viles, J.H. *J Biol Chem* 2004, 279, 18169-18177.
- [23] Syme, C.D.; Viles, J.H. *Biochim Biophys Acta* 2006, 1764, 246-256.
- [24] Ma, Q.F.; Hu, J.; Wu, W.H.; Liu, H.D.; Du, J.D.; Fu, Y.; Wu, Y.W.; Lei, P.; Zhao, Y.F.; Li, Y.M. *Biopolymers* 2006, 83, 20-31.

- [25] Dong, J.; Shokes, J.E.; Scott, R.A.; Lynn, D.G. *J Am Chem Soc* 2006, 128, 3540-3542.
- [26] Stellato, F.; Menestrina, G.; Dalla Serra, M.; Potrich, C.; Tomazzolli, R.; Meyer-Klaucke, W.; Morante, S. *Eur Biophys J* 2006, 35, 340-351.
- [27] Lee, P.A.; Citrin, P.H.; Eisenberg, P.; Kinkaid, B.M. *Rev Mod Phys* 1981, 53, 769-806.
- [28] Meneghini, C.; Morante, S. *Biophys J* 1998, 75, 1953-1963.
- [29] Morante, S.; Gonzalez-Iglesias, R.; Potrich, C.; Meneghini, C.; Meyer-Klaucke, W.; Menestrina, G.; Gasset, M. *J Biol Chem* 2004, 279, 11753-11759.
- [30] Redecke, L.; Meyer-Klaucke, W.; Koker, M.; Clos, J.; Georgieva, D.; Genov, N.; Echner, H.; Kalbacher, H.; Perbandt, M.; Bredehorst, R.; Voelter, W.; Betzel, C. *J Biol Chem*, 2005, 280, 13987-13992.
- [31] Mentler, M.; Weiss, A.; Grantner, K.; Del Pino, P.; Deluca, D.; Fiori, S.; Renner, C.; Meyer-Klaucke, W.; Moroder, L.; Bertsch, U.; Kretzschmar, H.A.; Tavan, P.; Parak, F.G. *Eur Biophys J* 2005, 34(2), 97-112.
- [32] Del Pino, P.; Weiss, A.; Bertsch, U.; Renner, C.; Mentler, M.; Grantner, K.; Fiorino, F.; Meyer-Klaucke, W.; Moroder, L.; Kretzschmar, H.A.; Parak, F.G. *Eur Biophys J* 2007, 36, 239-252.
- [33] Benfatto, M.; Natoli, C.R.; Bianconi, A.; Garcia, J.; Marcelli, A.; Fanfoni, M.; Davoli, I. *Phys Rev* 1986, B34, 5774-5781.
- [34] Bianconi, A.; Congiu-Castellano, A.; Dell'Ariceia, M.; Giovannelli, A.; Morante, S.; Burattini, E.; Durham, P.J. *Proc Natl Acad Sci USA* 1986, 83, 7736-7740.
- [35] Zirah, S.; Kozin, S.A.; Mazur, A.K.; Blond, A.; Cheminant, M.; Ségalas-Milazzo, I.; Debey, P.; Rebuffat, S. *J Biol Chem* 2006, 281, 2151-2161.
- [36] Danielsson, J.; Pierattelli, R.; Banci, L.; Graslund, A. *FEBS J* 2007, 274, 46-59.
- [37] Minicozzi, V.; Stellato, F.; Comai, M.; Dalla Serra, M.; Potrich, C.; Meyer-Klaucke, W.; Morante, S. *J Biol Chem* 2008, to be published.
- [38] Rossi, G.C. hep-th/0607211 and references therein.
- [39] Car, R.; Parrinello, M. *Phys Rev Lett* 1985, 55, 2471-2474.
- [40] Payne, M.C.; Teter, M.P.; Allan, D.C.; Arias, T.A.; Joannopoulos, J.D. *Rev Mod Phys* 1992, 64, 1045-1097.
- [41] Mark, D.; Hutter, J. *Modern Methods and Algorithms of Quantum Chemistry*, Grotendorst J. Ed.; John von Neumann Institute for Computing, Jülich, <http://www.fz-juelich.de/nic-series>.

- [42] Furlan, S.; La Penna, G.; Guerrieri, F.; Morante, S.; Rossi, G.C. *J Biol Inorg Chem* 2007, 12, 571-583.
- [43] Furlan, S.; La Penna, G.; Guerrieri, F.; Morante, S.; Rossi, G.C. *Eur Biophys J* 2007, 36, 841-845.
- [44] <http://www.cineca.it/>
- [45] <http://www.centrofermi.it/>
- [46] <http://www.ect.it/>
- [47] <http://www.cerm.it/>
- [48] <http://www.lrz-muenchen.de/>
- [49] Parr, R.G.; Yang, W. *Density Functional Theory of Atoms and Molecules*; Oxford University Press: Oxford, 1989;
Dreizler, R.M.; Gross, E.K.U. *Density functional theory*; Springer-Verlag: Berlin, 1990;
Fiolhais, C.; Nogueira, F.; Marques, M.A.L. *Primer in Density Functional Theory, Lecture Notes in Physics*; Springer-Verlag: Berlin, 2003;
Sousa, S.F.; Fernandes, P.A.; Ramos, M.J. *J. Phys. Chem. A* 2007, 111, 10439-10452.
- [50] Gao, J. *Chem Phys Lett* 1996, 263, 100-106;
Bash, P.A.; Ho, L.L.; MacKerell, A.D.J.; Levine, D.; Hallstrom, P. *Proc Natl Acad Sci USA* 1996, 93, 3698-3703;
Field, M.J.; Bash, P.A.; Karplus, M. *J Comp Chem* 1990, 11, 700-733,
Freindorf, M.; Gao, J. *J Comp Chem* 1996, 17, 386-395;
Gao, J. *Acc Chem Res* 1996, 29, 298-305;
Gao, J.; Amara, P.; Alhambra, C.; Field, M.J. *J Phys Chem* 1998, A102, 4714-4721;
Reuter, N.; Dejaegere, A.; Maignet, B.; Karplus, M. *J Phys Chem* 2000, A104, 1720-1735.
- [51] Pushie, M.J.; Rauk, A. *J Biol Inorg Chem* 2003, 8, 53-65.
- [52] Franzini, E.; De Gioia, L.; Fantucci, P.; Zampella, G. *Inorg Chem Comm* 2003, 6, 650-653.
- [53] Cox, D.L.; Pan, J.; Singh, R.R.P. *Biophys J Lett* 2006, 91, L11.
- [54] Carloni, P.; Blochl, P.; Parrinello, M. *J Phys Chem* 1995, 99, 1338-1348;
Hutter, J.; Carloni, P.; Parrinello, M. *J Am Chem Soc* 1996, 118, 8710-8712;
Carloni, P. *Quant Struct Act Relat* 2002, 21, 166-172;
Piana, S.; Bucher, D.; Carloni, P.; Rothlisberger, U. *J Phys Chem* 2004, B108, 11139-11149;
Sharma, M.; Resta, R.; Car, R. *Phys Rev Lett* 2005, 95, 187401-1-187401-4.

- [55] <http://www.embl.org/>
- [56] Lee, P.A.; Pendry, J.B. *Phys Rev* 1975, 11, 2795-2811.
- [57] Gurman, S.J.; Binsted, N.; Ross, I. *J Phys* 1986, C19, 1845-1861.
- [58] Koningsberger, D.C. and Prins, R. Eds.; *X-ray Absorption. Principles, applications, techniques of EXAFS, SEXAFS and XANES*; John Wiley & Sons: 1988, and references quoted therein.
- [59] Rehr, J.J.; Albers, R.C. *Phys Rev* 1990, B41, 8139-8149.
- [60] Jacquamet, L.; Aberdam, D.; Adrait, A.; Hazemann, J.L.; Latour, J.M.; Michaud-Soret, I. *Biochemistry* 1998, 37, 2564-2571.
- [61] Binsted, N. EXCURV98: CCLRC Daresbury Laboratory computer program, 1998.
- [62] Castagnetto, J.M.; Hennessy, S.W.; Roberts, V.A.; Getzoff, E.D.; Tainer, J.A.; Pique, M.E. *Nucleic Acids Res* 2002, 30, 379-382.
- [63] Binsted, N.; Strange, R.W.; Hasnain, S.S. *Biochemistry* 1992, 31, 12117-12125.
- [64] Kowalik-Jankowska, T.; Ruta, M.; Wisniewska, K.; Lankiewicz, L. *J Inorg Biochem* 2003, 95, 270-282.
- [65] Karr, J.W.; Akintoye H.; Kaupp, L.J.; Szalai, V.A. *Biochemistry* 2005, 44, 5478-5497.
- [66] Karr, J.W.; Szalai, V.A. *J Am Chem Soc.* 2007, 129, 3796-3797.
- [67] Miura, T.; Suzuki, K.; Kohata, N.; Takeuchi, H. *Biochemistry* 2000, 39, 7024-7031.
- [68] Martonak, R.; Laio, A.; Parrinello, M. cond-mat/0211551;
Kuo, I-F.W.; Mundy, C.J.; McGrath, M.J.; Siepmann, J.I.; VandeVondele, J.; Sprik, M.; Hutter, J.; Chen, B.; Klein, M.L.; Mohamed, F.R.; Krack, M.; Parrinello, M. *J Phys Chem* 2004, B108, 12990-12998;
Aktah, D.; Passerone, D.; Parrinello, M. *J Phys Chem*, 2004, A108, 848-854;
Kühne, T.D.; Krack, M.; Mohamed, F.R.; Parrinello, M. *Phys Rev Lett* 2007, 98, 066401-1-066401-4.
- [69] Ewald, P.P. *Ann Phys* 1921, 64, 253-287;
Allen, M.P.; Tildesley, D.J. *Computer simulation of liquids*; Clarendon Press: New York, USA, 1988;
Darden, T.; York, D.; Pedersen, L. *J Chem Phys* 1993, 98, 10089-10092;
Essmann, U.; Perera, L.; Berkowitz, M.L.; Darden, T.; Lee, H.; Pedersen, L.G. *J Chem Phys* 1995, 103, 8577-8592.

- [70] Kirschner, D.A.; Abraham, C.; Selkoe, D.J. *Proc Natl Acad Sci USA* 1986, 83, 503-507;
Kirschner, D.A.; Inouye, H.; Duffy, L.K.; Sinclair, A.; Lind, M.; Selkoe, D.J. *Proc Natl Acad Sci USA* 1987, 84, 6953-6957;
Sunde, M.; Serpell, L.C.; Bartlam, M.; Fraser, P.E.; Bepys, M.B.; Blake, C.C.F. *J Mol Biol* 1997, 273, 729-739;
Balbach, J.J.; Ishii, Y.; Antzutkin, O.N.; Leapman, R.D.; Rizzo, N.W.; Dyda, F.; Reed, J.; Tycko, R. *Biochemistry* 2000, 39, 13748-13759.
- [71] Ma, B.; Nussinov, R. *Proc Natl Acad Sci USA* 2002, 99, 14126-14131;
Rohrig, U.F.; Laio, A.; Tantalo, N.; Parrinello, M.; Petronzio, R. *Biophys J* 2006, 91, 3217-3229.
- [72] Lambert, M.P.; Barlow, A.K.; Chromy, B.A.; Edwards, C.; Freed, R.; Liosatos, M.; Morgan, T.E.; Rozovsky, I.; Trommer, B.; Viola, K.L.; Wals, P.; Zhang, C.; Finch, C.E.; Krafft, G.A.; Klein, W.L. *Proc Natl Acad Sci USA* 1998, 95, 6448-6453.
- [73] Chromy, B.A.; Nowak, R.J.; Lambert, M.P.; Viola, K.L.; Chang, L.; Velasco, P.T.; Jones, B.W.; Fernandez, S.J.; Lacor, P.N.; Horowitz, P.; Finch, C.E.; Krafft, G.A.; Klein, W.L. *Biochemistry* 2003, 42, 12749-12760.
- [74] Klein, W.L. *Protein Misfolding, Aggregation and Conformational diseases, Part A*, Uversky, V.N. and Fink, A.L. Eds.; Springer, 2006, 61-81.
- [75] Giannozzi, P.; de Angelis, F.; Car, R. *J Chem Phys* 2004, 120, 5903-5915.
- [76] Baroni, S.; Dal Corso, A.; de Gironcoli, S.; Giannozzi, P.; Cavazzoni, C.; Balabio, G.; Scandolo, S.; Chiarotti, G.; Focher, P.; Pasquarello, A.; Laasonen, K.; Trave, A.; Car, R.; Marzari, N.; Kokalj, A. <http://www.pwscf.org/>.
- [77] Vanderbilt, D. *Phys Rev* 1990, B41, 7892-7895.
- [78] Perdew, J.P.; Burke, K.; Ernzerhof, M. *Phys Rev Lett* 1996, 77, 3866-3868.
See also: Zhang, Y.; Yang, W. *Phys Rev Lett* 1998, 80, 890 and the reply by Perdew, J.P.; Burke, K.; Ernzerhof, M. at page 891 of the same issue.
- [79] Tickler, A.K.; Smith, D.G.; Ciccotosto, G.D.; Tew, D.J.; Curtain, C.C.; Carington, D.; Masters, C.L.; Bush, A.I.; Cherny, R.A.; Cappa, R.; Wade, J.D.; Barnham, K.J. *J Biol Chem* 2005, 280, 13355-13363.
- [80] Stryer, L. *Biochemistry*, Freeman and Company: New York, USA, 1995.
- [81] <http://www.gromacs.org/>
- [82] Curtain, C.C.; Ali, F.; Volitakis, I.; Cherny, R.A.; Norton, R.S.; Beyreuther, K.; Barrow, C.J.; Masters, C.L.; Bush, A.I.; Barnham, K.J. *J Biol Chem* 2001, 276, 20466-20473.
- [83] Smith, D.G.; Cappai, R.; Barnham, K.J. *Biochimica et Biophysica Acta* 2007, 1768, 1976-1990.

- [84] Raffa, D.F.; Gómez-Balderas, R.; Brunelle, P.; Rickard, G.A.; Rauk, A. *J Biol Inorg Chem* 2005, 10, 887-902.
- [85] Raffa, D.F.; Rauk, A. *J Phys Chem B* 2007, 111, 3789-3799.
- [86] Nosé, S. *Molec Phys* 1984, 52, 255-268;
Hoover, W.G. *Phys Rev A* 1985, 31, 1695-1697.
- [87] Frenkel, D.; Smit, B. *Understanding Molecular Simulation - From Algorithms to Applications*; Academic Press: San Diego, 1996.